Journal of Pharmaceutical Analysis 13 (2023) 1024–1040

Contents lists available at ScienceDirect

Journal of Pharmaceutical Analysis

journal homepage: www.elsevier.com/locate/jpa

Original article

Gut microbiota-based pharmacokinetic-pharmacodynamic study and molecular mechanism of specnuezhenide in the treatment of colorectal cancer targeting carboxylesterase

Hang Yu [1], Hui Xu [1], Xinyu Yang, Zhengwei Zhang, Jiachun Hu, Jinyue Lu, Jie Fu, Mengmeng Bu, Haojian Zhang, Zhao Zhai, Jingyue Wang, Jiandong Jiang*, Yan Wang**

State Key Laboratory of Bioactive Substance and Function of Natural Medicines, Institute of Materia Medica, Chinese Academy of Medical Sciences/Peking Union Medical College, Beijing, 100050, China

ARTICLE INFO

Article history:
Received 12 February 2023
Received in revised form
15 June 2023
Accepted 25 June 2023
Available online 28 June 2023

Keywords:
Specnuezhenide
Pharmacokinetics
Tumor
Gut microbiota
Fungi
Metabolism

ABSTRACT

Specnuezhenide (SNZ) is among the main components of Fructus Ligustri Lucidi, which has anti-inflammation, anti-oxidation, and anti-tumor effect. The low bioavailability makes it difficult to explain the mechanism of pharmacological effect of SNZ. In this study, the role of the gut microbiota in the metabolism and pharmacokinetics characteristics of SNZ as well as the pharmacological meaning were explored. SNZ can be rapidly metabolized by the gut microbiome, and two intestinal bacterial metabolites of SNZ, salidroside and tyrosol, were discovered. In addition, carboxylesterase may be the main intestinal bacterial enzyme that mediates its metabolism. At the same time, no metabolism was found in the incubation system of SNZ with liver microsomes or liver homogenate, indicating that the gut microbiota is the main part involved in the metabolism of SNZ. In addition, pharmacokinetic studies showed that salidroside and tyrosol can be detected in plasma in the presence of gut microbiota. Interestingly, tumor development was inhibited in a colorectal tumor mice model administered orally with SNZ, which indicated that SNZ exhibited potential to inhibit tumor growth, and tissue distribution studies showed that salidroside and tyrosol could be distributed in tumor tissues. At the same time, SNZ modulated the structure of gut microbiota and fungal group, which may be the mechanism governing the antitumoral activity of SNZ. Furthermore, SNZ stimulates the secretion of short-chain fatty acids by intestinal flora in vitro and in vivo. In the future, targeting gut microbes and the interaction between natural products and gut microbes could lead to the discovery and development of new drugs.

1. Introduction

Fructus Ligustri Lucidi (FLL) is a traditional Chinese medicine, derived from the dry ripe fruit of *Ligustrum lucidum* Ait. According to the Pharmacopoeia of the People's Republic of China, Fructus Ligustri Lucidi (FLL) has several traditional properties and uses. It is believed to nourish Yin (a concept related to coolness and moisture in the body) and promote longevity. FLL is also known for its ability to nourish the liver and kidneys, clear heat, improve eyesight, and help with the growth of black hair. It is commonly used in the treatment of conditions like liver and kidney Yin deficiency, which can cause symptoms such as dizziness, tinnitus, and weakness in the waist and knees. FLL is also used for addressing internal heat and thirst, as well as hot flashes. Additionally, FLL is an important ingredient in a traditional Chinese medicine called Erzhi pill, which is known for its potential to tonify the liver and kidneys, nourish Yin, and stop bleeding. It is reported that FLL contains a variety of compounds such as triterpenes, iridoids, phenylethanol glycosides, and flavonoids [1–3]. Modern pharmacological studies have revealed that FLL exhibits a variety of pharmacological activities, including antioxidant, anti-inflammatory and analgesic, hepatoprotective, anti-osteoporotic, immunomodulatory, hypoglycemic, and hypolipidemic, antibacterial and antiviral activities [4–10]. Iridoids are important chemical constituents in FLL. Among them, specnuezhenide (SNZ) is a quality marker of FLL in the Pharmacopoeia of the People's Republic of China. SNZ exhibits pharmacological effects such as inhibiting oxidative stress, regulating immunity, protecting liver and kidney, and exerting anti-tumor effects [11–14]. However, the bioavailability of iridoids is often not high, and the bioavailability of SNZ is only approximately

Peer review under responsibility of Xi'an Jiaotong University.
* Corresponding author.
** Corresponding author.
E-mail addresses: jiang.jdong@163.com (J. Jiang), wangyan@imm.ac.cn (Y. Wang).
[1] Both authors contributed equally to this work.

https://doi.org/10.1016/j.jpha.2023.06.012

1%–2% [15], which suggests that these compounds undergo extensive metabolism after oral administration. The poor oral absorption and low bioavailability of SNZ make it difficult to explain the underlying mechanisms of its pharmacological effects. In fact, low bioavailability is a common problem with many potent natural compounds.

Intestinal microbes consist of bacteria, fungi, and bacteriophages that inhabit in the gut, and participate in a variety of important physiological functions of the host, such as material exchange, energy metabolism, and gene communication [16,17]. At the same time, gut microbes in direct contact with the external environment can lead the response to external stimuli. Therefore, the biotransformation and bioavailability of oral natural medicines are also affected by gut microbes [18]. Unlike liver metabolism, gut microbes are rich in many enzymes related to hydrolysis and reduction reactions, and thus mediate unique types of biotransformation [18,19]. Additionally, gut microbes can produce various endogenous secondary metabolites, such as bacteria, which can produce short-chain fatty acids, trimethylamine, indole propionic acid [20–23], etc., and fungi, which can produce ethanol, antimicrobial peptides [24–26], etc. As a result, the occurrence and development of metabolic syndrome, autoimmune diseases, tumors, inflammation, emotional cognitive dysfunction, and other diseases is affected [27–31]. Therefore, we can infer that gut microbes are important mediators of drug metabolism, diseases, and the body. It is of vital importance to illustrate the role of the gut microbiota in the metabolism and pharmacokinetics characteristics of SNZ, and uncover the pharmacological meaning of it.

Cancer is among the top global public health problems and is currently the second leading cause of death in the United States [32]. Among cancers, the incidence of colorectal tumor has ranked the third after prostate tumor (male)/breast cancer (female), and lung/bronchial tumor, and gradually showed a trend of incidence in younger individuals [33]. In 2022, the mortality rate of colorectal tumors is expected to exceed 8%–9% [32]. Therefore, developing more efficient and safer treatment methods is a top priority. Like many diseases, the formation of colorectal tumors is multifactorial. At present, the pathogenesis of colorectal tumors includes genetic factors, aging, overweight and obesity, smoking and drinking, low-fiber and high-fat diet, diabetes and insulin resistance, immunity disorder [34], etc. In recent years, gut microbes have been reported to play an important role in the occurrence and development of tumors [35,36]. For example, *Clostridium difficile* and *Fusobacterium nucleatum* are closely related to colorectal tumors [16], while *Malassezia* spp., a fungal genus in human gut, can promote the development of pancreatic cancer through mannose-binding lectins [37]. Novel treatments targeting gut microbes appear promising.

In this study, the role of gut microbiota in metabolism and pharmacokinetics characteristics was investigated. SNZ was rapidly metabolized by gut microbiota. Salidroside and tyrosol are the characteristic metabolites of SNZ by gut bacteria after hydrolyzing the carboxyl ester bond. The carboxylesterase in intestinal flora was found to be one of the main reasons for the low bioavailability of SNZ. At the same time, pharmacokinetic studies showed that the metabolic behavior of SNZ and two metabolites in mice was closely related to the intestinal flora. Notably, tumor growth was significantly inhibited after oral administration of SNZ in colorectal tumor mice, and this effect was dependent on gut microbes. Tissue distribution studies also showed that salidroside and tyrosol were distributed in the tumor site, suggesting that salidroside and tyrosol may be the effective substances of SNZ against cancer. At the same time, SNZ regulated the composition of gut microbiota and fungi in mice, and in vitro and in vivo experiments demonstrated that SNZ can stimulate the intestinal flora to secrete short-chain fatty acids. In conclusion, gut microbes are the key mediators and targets of the pharmacodynamics of SNZ, providing new insights for the discovery and development of new anticancer drugs and new targets.

2. Experimental

2.1. Chemicals and reagents

SNZ was purchased from Solarbio Biotechnology, Co., Ltd. (Beijing, China). Salidroside and tyrosol were purchased from Solarbio Biotechnology, Co., Ltd.. Glipizide as internal standard (IS) was purchased from Solarbio Biotechnology, Co., Ltd.. Formic acid and acetic acid were purchased from Merck (Darmstadt, Germany). Phosphoric acid, propionic acid, and butyric acid was purchased from Sigma-Aldrich (St. Louis, MO, USA). The purity of the above chemicals is greater than 98%. Chromatography grade methanol and acetone were obtained from Thermo Fisher Scientific Inc. (Fair Lawn, NJ, USA). Phosphate buffered saline (PBS), *bis-p*-nitrophenyl phosphate (BNPP), urethane, erythromycin, oxytetracycline, cefadroxil, and anaerobic medium were also supplied by Solarbio Biotechnology, Co., Ltd.. Other chromatographic reagents were obtained from domestic reagent companies. Inflammatory factors detection kits of tumor necrosis factor-α (TNF-α), IL-6, and interleukin-1β (IL-1β) were purchased from Nanjing Jiancheng Bioengineering Institute (Nanjing, China).

2.2. Instruments and methods

The high performance liquid chromatograph coupled with a triple quadrupole mass spectrometer, LC/MS-8060 (Shimadzu Corporation, Kyoto, Japan), was used for the quantitative detection of SNZ and its metabolites. A shaking incubator was purchased from Longyue Instrument Co., Ltd. (Shanghai, China). A WH-681 vortex mixer was purchased from Jintan Shenglan Instrument Manufacturing Co., Ltd. (Jintan, China). The refrigerated high-speed centrifuge was purchased from Eppendorf (Hamburg, Germany).

Chromatography separation was performed using an Alltima C_{18} column (4.6 mm × 250 mm, 5 mm; GRACE®, Chicago, IL, USA) at a flow rate of 0.4 mL/min. And the column temperature was maintained at 40 °C. The mobile phase was deionized water (eluent A) with methanol (eluent B). The gradient programming of the solvent system was initially at 20% B, 20%–70% B for 0–5 min, 70%–95% B for 5–11 min, and 95%–20% B for 11–17 min. The autosampler temperature was set to 4 °C.

Mass spectrometry (MS) was carried out using multiple reaction monitoring mode (MRM). The following ion pairs were monitored: SNZ (*m/z*, negative MRM) of 685.15 → 523.30 (Q1 pre bias: 26.0 V, CE: 19.0 V, Q3 pre bias: 36.0 V, dwell time: 50 ms), salidroside (*m/z*, negative MRM) of 299.10 → 119.10 (Q1 pre bias: 12.0 V, CE: 13.0 V, Q3 pre bias: 22.0 V, dwell time: 50 ms), tyrosol (*m/z*, negative MRM) of 137.40 → 105.90 (Q1 pre bias: 14.0 V, CE: 17.0 V, Q3 pre bias: 11.0 V, dwell time: 50 ms), and glipizide (IS, *m/z*, negative MRM) of 444.25 → 319.10 (Q1 pre bias: 18.0 V, CE: 18.0 V, Q3 pre bias: 24.0 V, dwell time: 50 ms). The nebulizing gas flow rate was 3.0 L/min, the drying gas flow rate was 10 L/min, and the heating gas flow rate was 10 L/min.

High performance liquid chromatography (HPLC) coupled with an ion trap time-of-flight tandem MS (HPLC/MS^n-IT-TOF) from Shimadzu Corporation was implemented to identify the metabolites of SNZ. The analytes were separated using an Alltima C_{18} column (4.6 mm × 250 mm, 5 mm; GRACE®) at a flow rate of 0.4 mL/min, and the column temperature was maintained at 40 °C. The mobile phase was deionized water (eluent A) with methanol (eluent B). The gradient programming of the solvent system was initially at 20% B, 20%–70% B for 0–5 min, 70%–95% B for 5–11 min, and 95%–20% B for 11–17 min. The autosampler temperature was

set to 4 °C. The detection wavelength for photo-diode array was 254 nm. The MS conditions were set as follows: heating block temperature, 200 °C; nebulizing gas flow rate, 1.5 L/min; detector voltage, 1.76 kV; and collision energy, 70%. Automatic detection mode was used for fragmentation, with a primary *m/z* ratio ranging from 50 to 800 and a secondary *m/z* ratio ranging from 50 to 800.

The gas chromatograph (GC-2020) was purchased from Shimadzu Corporation. Quantification of short-chain fatty acid by gas chromatography was performed as described previously [38]. A high polarity Alltech capillary column (AT-WAX, 30 m × 0.25 mm × 0.25 μm; Alltech Cooperation, Chicago, IL, USA) was used for separation with parameters as follows: nitrogen flow, 1.27 mL/min; purge flow, 3.0 mL/min; total pressure, 105.0 kPa; injection port, 230 °C; and flame ionization detector, 250 °C, respectively. The temperature programming started with 80 °C for 1 min, and linearly increased to 130 °C at the rate of 5 °C/min, and maintained for 5 min.

2.3. Biotransformation of SNZ in vitro

2.3.1. Metabolism of SNZ by intestinal bacteria in vitro

In vitro co-incubation experiment of SNZ and gut microbiota was conducted as previously report [39,40]. Briefly, the intestinal contents of 8-week-old male Balb/c mice were collected, and then mixed with the anaerobic medium at a weight-to-volume ratio of 1:30 to obtain the incubation system of intestinal bacteria. After mixing evenly, the incubation system was filled with N_2 and stored at 37 °C with pre-incubation for 30 min. Next, 1.0 mg of SNZ was accurately weighed, and then methanol was added to obtain a 1.0 mg/mL stock solution. 10 μL of the SNZ stock solution was taken to 990 μL of the intestinal bacteria culture medium. The incubation system was filled with N_2 to maintain an anaerobic state. The final concentration of SNZ in the incubation system was 10 μg/mL. At the same time, the inactivated intestinal bacteria incubation system medium was used as a negative control. The incubation experiment was carried out twice. In the first experiment, the above-mentioned intestinal bacteria incubation system was incubated in a shaker at 37 °C and 200 rpm for 0, 1, 2, 6, 12, and 24 h, respectively. In the second experiment, the above-mentioned intestinal bacteria incubation system was incubated at 37 °C and 200 rpm in a shaker for 0, 15, 30, 60, 90, and 120 min, respectively. When the incubation reaction was terminated, 3-fold volume of methanol solution containing 100 ng/mL of glipizide was added, and then the mixture was vortexed for 30 s and centrifuged at 14,000 rpm for 10 min in a refrigerated centrifuge at 4 °C. 6 μL of the supernatant was injected into HPLC-MS/MS for quantitative analysis. At the same time, 10 μL of supernatant was injected into HPLC-MS^n-IT-TOF for the identification of metabolites.

Then, 1 mg/mL of SNZ methanol solution was gradually diluted to a series of stock solutions with concentrations of 500, 100, 20, 5, 1, 0.5, and 0.1 μg/mL, respectively. SNZ standard samples were composed of a series of 10 μL of SNZ stock solutions and 990 μL of inactivated medium, for quantification of the metabolism of SNZ. A mixed solution containing 1 mg/mL of salidroside, and 1 mg/mL of tyrosol was prepared. Methanol was gradually added to obtain a series of mixed stock solutions of 500, 100, 50, 20, 5, 1, 0.5, and 0.1 μg/mL. Mixed standard samples were composed of a series of 10 μL mixed stock solutions and 990 μL inactivated medium, for quantification of metabolites of SNZ. The rest of the sample processing steps were the same as above.

2.3.2. Metabolism of SNZ in liver microsome and the liver homogenate in vitro

The liver microsome incubation system was consisted of the following: 5 μL of mice liver microsomes (20 mg/mL), 2 μL of SNZ (1 mM), 20 μL of reduced nicotinamide adenine dinucleotide phosphate (NADPH, 1.3 mM), and 0.05 mM Tris/HCl (pH = 7.4), with a total volume of 200 μL. The negative control group without liver microsomes consists of 2 μL of SNZ (1 mM), 20 μL of NADPH (1.3 mM), and 0.05 mM Tris/HCl (pH = 7.4), with a total volume of 200 μL. The incubation was conducted in a shaking incubator at 37 °C and 800 rpm with supply of oxygen. After the incubation, 3-fold volume of glipizide methanol solution (100 ng/mL) was added to the incubation system and mixed to stop the reaction at 0, 15, 30, 60, 90, and 120 min. After centrifugation at 14,000 rpm in a refrigerated centrifuge at 4 °C for 10 min, 6 μL of the supernatant was injected for HPLC-MS/MS analysis.

Liver homogenate was prepared by homogenizing freshly collected mice livers and adding ice-cold normal saline with the ratio of 1:3 (*m*/*V*). The liver homogenate incubation system was consisted as follows: 2 μL of SNZ (1 mM) and 198 μL of freshly prepared liver homogenate, with a total volume of 200 μL. The negative control group without liver homogenate consists of 2 μL of SNZ (1 mM) and 198 μL of normal saline, with a total volume of 200 μL. Incubation was conducted in a shaking incubator at 37 °C and 800 rpm with supply of oxygen. After the incubation, 3-fold volume of glipizide methanol solution (100 ng/mL) was added to the incubation system and mixed to stop the reaction at 0, 15, 30, 60, 90, and 120 min. After centrifugation at 14,000 rpm in a refrigerated centrifuge at 4 °C for 10 min, 10 μL of the supernatant was injected for HPLC-MS/MS analysis.

Then, 1 mg/mL of SNZ methanol solution was gradually diluted to a series of stock solutions with concentrations of 500, 100, 20, 5, 1, 0.5, and 0.1 μg/mL, respectively. SNZ standard samples were composed of a series of 2 μL of SNZ stock solutions and 198 μL of 0.05 mM Tris/HCl (pH = 7.4) or 198 μL of inactivated liver homogenate for the detection of SNZ. The rest of the sample processing steps were the same as above.

2.3.3. Determination of short-chain fatty acid in vitro

The intestinal contents of 8-week-old male Balb/c mice were collected, and the intestinal contents were mixed with the anaerobic medium at a weight-to-volume ratio of 1:30 to obtain the incubation system of intestinal bacteria. After mixing evenly, the incubation system was filled with N_2 and stored at 37 °C to pre-incubate for 30 min.

Next, 1.0 mg of SNZ was accurately weighed, and then methanol was added to obtain a 1.0 mg/mL stock solution. 10 μL of the SNZ stock solution was taken to 990 μL of the intestinal bacteria culture medium. The incubation system was filled with N_2 to maintain an anaerobic state. The final concentration of SNZ in the incubation system was 10 μg/mL. At the same time, 10 μL of methanol was added to 990 μL of intestinal bacteria incubation system medium as a negative control. In the incubation experiment, the above-mentioned intestinal bacteria incubation system was incubated in a shaker at 37 °C and 200 rpm for 0, 1, 2, 6, 12, and 24 h, respectively.

At the end of the incubation reaction, acetone (with 1% (*V*/*V*) phosphoric acid) for short-chain fatty acid extraction was added. The mixture was centrifuged at 14,000 rpm for 10 min at 4 °C and the supernatant was directly injected for analysis.

2.4. Carboxylesterase-mediated transformation of SNZ

2.4.1. SNZ molecular virtual docking analysis

Docking analysis between SNZ and carboxylesterase was conducted using Discovery Studio Client software (v16.1.0.15350). Carboxylesterase 1AUO was used as the model enzyme which was derived from *Pseudomonas fluorescens*. The crystal structure of carboxylesterase 1AUO was obtained from the Protein Data Bank (PDB) database and the docking between SNZ and carboxylesterase was performed using the CDOCKER approach as the docking

algorithm for our docking study. During the docking process, the protein was kept rigid while the ligands were treated as fully flexible and a final minimization step was used to refine the docked positions. In addition, the parameters were set to the default values.

2.4.2. Effect of BNPP inhibition on the transformation of SNZ

Consistent with the above steps in Section 2.3.1, the carboxylesterase inhibitor BNPP (1, 5, and 10 mM) was added to the culture system containing SNZ with a final concentration of 10 μg/mL. Then, the cultures were incubated at 37 °C for 0, 15, 30, 60, 90, and 120 min. The intestinal culture system without BNPP was used as a control group.

2.5. Tumor cell lines and cell culture

The murine colorectal cancer cell line colon 26 was originally obtained from Guangzhou Jeniobio Biotechnology Co., Ltd. (Guangzhou, China). This cell line was cultured at 37 °C in a humidified atmosphere containing 5% CO_2 in Roswell Park Memorial Institute-1640 medium (pH 7.4; Invitrogen, Carlsbad, NM, USA) supplemented with 100 units/mL penicillin and 100 mg/mL streptomycin (Gibco, St. Louis, MO, USA) and 10% (*V*/*V*) fetal bovine serum (Invitrogen).

2.6. Animals

Male Balb/c mice (20–25 g) aged 7–8 weeks were supplied by Vitalriver (Beijing, China). The animals were placed in a room with temperature of 22–24 °C, humidity of 45%, and a 12-h light/dark cycle. Before the experiment, mice were fasted for 12 h but had free access to water. All experiments were conducted in accordance with institutional and ethics guidelines and were approved by the Laboratories Institutional Animal Care and Use Committee of the Chinese Academy of Medical Sciences and Peking Union Medical College (Approve No.: 00009209).

Colon 26 cells (2×10^6 cells/mouse) were implanted intrarectally with a micropipette inserted 2 cm into the anus of the mice. Successful tumor models were used at one week after implantation of tumor cells for pharmacokinetics study.

2.7. Pharmacokinetics and tissue distribution of SNZ mediated by the gut microbiota in Balb/c mice

2.7.1. Pharmacokinetics and tissue distribution of SNZ in Balb/c mice

The animals were fasted overnight but had free access to water before pharmacokinetics studies. Five Balb/c mice and five tumor bearing mice were orally administered of SNZ (109.2 mg/kg). 60 μL of blood from the orbital vein was collected at 0, 1, 5, 10, 20, 40, 60, 90, 120, 240, and 480 min after drug administration. Plasma was collected after centrifugation at 5,000 rpm and immediately stored at −80 °C before analysis.

A mixed solution containing 1 mg/mL of SNZ, 1 mg/mL of salidroside, and 1 mg/mL of tyrosol was prepared. Methanol was gradually added to obtain a series of mixed stock solutions of 500, 100, 50, 20, 5, 1, 0.5, and 0.1 μg/mL. SNZ standard samples were composed of a series of 2 μL of mixed stock solutions and 198 μL of blank plasma for the detection of SNZ, salidroside, and tyrosol.

90 μL of methanol solution containing glipizide (100 ng/mL) was added to 30 μL of plasma, and then the mixture was vortexed for 1 min, and centrifuged at 14,000 rpm for 10 min. 6 μL of supernatant was injected in HPLC-MS/MS for analysis.

For tissue distribution study, the animals were fasted overnight but had free access to water before pharmacokinetics studies. Three tumor bearing mice were orally administered of SNZ (109.2 mg/kg). After 20 min, the mice were anesthetized with 20% (*V*/*V*) urethane, and after adequate perfusion with PBS, the liver, heart, spleen, lung, kidney, stomach, small intestine, colon, fat, testis, muscle, brain, and tumor tissues were collected and added with 3-fold volume of PBS before homogenization. 300 μL of methanol solution containing glipizide (100 ng/mL) was added to 100 μL of tissue homogenate, and then the mixture was vortexed for 1 min, and centrifuged at 14,000 rpm for 10 min. 6 μL of supernatant was injected in HPLC-MS/MS for analysis.

2.7.2. Pharmacokinetics and tissue distribution of SNZ in the pseudo-germfree (PGF) mice

Five Balb/c mice and five tumor bearing mice were orally administered erythromycin (200 mg/kg/day), oxytetracycline (200 mg/kg/day), and cefalexin (100 mg/kg/day) for three consecutive days to achieve PGF status. Mice feces were collected on day 3 post-treatment, and colony culture was performed on a nutrient agar culture medium to confirm the PGF status. After administration, pharmacokinetic experiments were performed. The animals were fasted overnight but had free access to water before pharmacokinetics studies. Five Balb/c mice and five tumor mice under PGF status were orally administered of SNZ (109.2 mg/kg). 60 μL of blood from the orbital vein was collected at 0, 1, 5, 10, 20, 40, 60, 90, 120, 240, and 480 min after drug administration. Plasma was collected after centrifugation at 5,000 rpm and immediately stored at −80 °C until analysis.

A mixed solution containing 1 mg/mL SNZ, 1 mg/mL salidroside, and 1 mg/mL tyrosol was prepared, respectively. Methanol was gradually added to obtain a series of mixed stock solutions of 500, 100, 50, 20, 5, 1, 0.5, and 0.1 μg/mL. SNZ standard samples were composed of a series of 2 μL of mixed stock solutions and 198 μL of blank plasma for the detection of SNZ, salidroside, and tyrosol.

90 μL of methanol solution containing glipizide (100 ng/mL) was added to 30 μL of plasma, and then the mixture was vortexed for 1 min, and centrifuged at 14,000 rpm for 10 min. 6 μL of supernatant was injected in HPLC-MS/MS for analysis.

For tissue distribution study, the animals were fasted overnight but free access to water before pharmacokinetics studies. Three tumor bearing mice under PGF state were orally administered of SNZ (109.2 mg/kg). After 20 min, the mice were anesthetized with 20% (*V*/*V*) urethane, and after adequate perfusion with PBS, the liver, heart, spleen, lung, kidney, stomach, small intestine, colon, fat, testis, muscle, brain, and tumor tissues were collected and added with 3-fold volume of PBS before homogenization. 300 μL of methanol solution containing glipizide (100 ng/mL) was added to 100 μL of tissue homogenate, and then the mixture was vortexed for 1 min and centrifuged at 14,000 rpm for 10 min. 6 μL of supernatant was injected in HPLC-MS/MS for analysis.

2.8. Exploration of antitumoral activity of SNZ

2.8.1. Antitumoral activity of SNZ

In order to explore the pharmacological effects of SNZ on colorectal tumors, a mouse colorectal tumor model was established, and after continuous oral administration for 10 days, the therapeutic effect of SNZ on colorectal tumors was evaluated.

In the pharmacology study of SNZ, the administration dose was set at 109.2 mg/kg. The main rationale of the chosen dosage is as follows. SNZ is one of the main components of traditional Chinese patent Erzhi pill. The adult daily dose of Erzhi pill is 18 g/60 kg for traditional use. To investigate the potential antitumoral activity of SNZ and Erzhi pill, 10 times of dosage was applied. According to the Pharmacopoeia of the People's Republic of China, the SNZ content in the Erzhi pill was not less than 4.0 mg/g. Based on the conversion of data from the adult therapeutic dose to the dose administered to

mice, the mice dose is 9.1 times higher than the adult dose. Therefore, the mice dose of SNZ is approximately 109.2 mg/kg.

A total of six groups ($n = 5$) were set up in the experiment: (1) normal group: healthy Balb/c mice were given normal saline daily; (2) normal PGF (NPGF) group: healthy Balb/c mice were given erythromycin 200 mg/kg, oxytetracycline 200 mg/kg, and cefadroxil 100 mg/kg daily to establish NPGF model, and administered normal saline daily; (3) tumor group: tumor mice were given normal saline daily; (4) SNZ group: model mice were given SNZ 109.2 mg/kg daily; (5) PGF tumor (TPGF) group: tumor mice were given erythromycin 200 mg/kg, oxytetracycline 200 mg/kg, and cefadroxil 100 mg/kg every day to establish a TPGF model, and administered normal saline daily; and (6) PGF tumor and SNZ (SNZ TPGF) group: tumor mice were given erythromycin 200 mg/kg, oxytetracycline 200 mg/kg, and cefadroxil 100 mg/kg daily to establish a PGF tumor model, and then PGF tumor mice were given SNZ 109.2 mg/kg daily.

At the end of the experiment, all experimental animals were sacrificed by anesthesia with 0.5 mL of 20% (*V*/*V*) urethane. Body weight was measured, feces were collected, and vital organs such as tumor tissue and spleen were collected. Inflammatory factors (TNF-α, IL-6, and IL-1β) content was determined according to the kit instructions.

2.8.2. Determination of short-chain fatty acid in feces of SNZ-treated mice

Fecal samples (about 0.2 g) were pretreated by dilution (weight (g): volume (μL) = 1:1000) in water. The mixture was centrifuged at 14,000 rpm for 10 min at 4 °C. Then, 100 μL of supernatant was added to acetone (with 1% (*V*/*V*) phosphoric acid) for short chain fatty acid extraction. The mixture was centrifuged at 14,000 rpm for 10 min at 4 °C and the supernatant was directly injected for analysis.

2.9. Analysis of microbial diversity

Mice feces were collected after 10 days of treatment. Microbial DNA in fecal samples was extracted using the E.Z.N.A.® Soil DNA Kit (Omega Biotek, Norcross, GA, USA) according to the instructions. The V3–V4 region of the microbial 16S ribosomal RNA (rRNA) gene was amplified with primer pairs 338F (5′-ACTCCTACGGGAGGCAGCAG-3′) and 806R (5′-GGACTACHVGGGTWTCTAAT-3′). Polymerase chain reaction (PCR) products were then extracted from 2% (*m*/*m*) agarose gels and purified using the AxyPrep DNA Gel Extraction Kit (Axygen Biosciences, Union City, CA, USA). Purified amplicons were sequenced using Illumina MiSeq (Illumina, Inc., San Diego, CA, USA) to analyze the diversity of bacterial groups in animal feces from each group. In addition, primer pairs for the microbial ITS-1 gene: 18S-F (5′-GTAAAAGTCGTAACAAGGTTTC-3′) and 5.8S-1R (5′-GTTCAAAGAYTCGATGATTCAC-3′) were used for amplification. PCR products were then extracted from 2% agarose gels and purified using the AxyPrep DNA Gel Extraction Kit (Axygen Biosciences). The purified amplicons were sequenced using Illumina MiSeq to analyze the diversity of the fungal group in animal feces from each group.

2.10. Statistical analysis

Statistical analyses were conducted using two-way analysis of variance and Student's *t*-test with GraphPad Prism Version 8 (GraphPad Software, La Jolla, CA, USA). The data are expressed as the means ± standard deviation. *P*-values less than 0.05 were considered statistically significant. DAS 3.0 (Shanghai, China) was used to calculate the plasma pharmacokinetic parameters.

3. Results

3.1. Gut microbiota plays an important role in the metabolism of SNZ

To investigate whether SNZ could interact with the gut microbiota to generate a unique metabolic profile, and demonstrate the unique role of the gut microbiota in drug metabolism, we compared the metabolic characteristics between the gut microbiota and the liver. A quantitative detection method for SNZ using HPLC-MS/MS

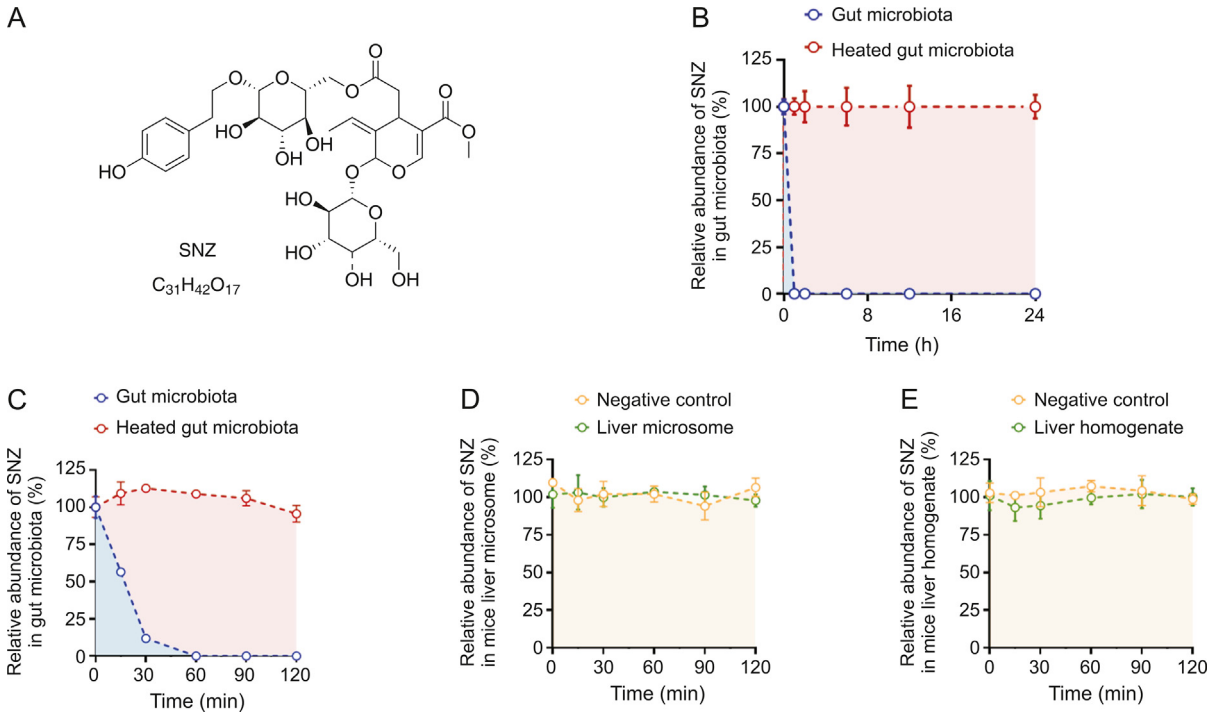

Fig. 1. Specnuezhenide (SNZ) could be metabolized in the gut microbiota. (A) The structural formula of SNZ. (B) The metabolic curve of SNZ by intestinal bacteria. (C) The metabolic characteristic of SNZ by gut microbiota in more precise spans of time. (D) The metabolic curve of SNZ by liver microsome. (E) The metabolic curve of SNZ by liver homogenate.

was first established to explore whether SNZ could be metabolized by gut microbiota. Fig. 1A shows the molecular structure of SNZ. The retention time of SNZ in this method was 11.5 min, and the glipizide (IS) was 14.4 min. Next, we incubated the mixture of cecum contents with SNZ (final concentration of 10 μg/mL) for 24 h to explore the metabolism of SNZ by gut microbiota. A double heat-inactivated cecum content mixture was used as a negative control to exclude the interference of environmental factors such as culture medium. Samples were collected at 0, 1, 2, 6, 12, and 24 h after incubation, and the content of SNZ in the system was detected by HPLC-MS/MS. As shown in Fig. 1B, SNZ disappeared rapidly in this system. Compared with the inactivated negative control, the parent drug concentration was completely consumed within 1 h, while the inactivated group maintained the original concentration at 24 h, indicating a strong metabolic effect of gut microbiota on SNZ. To further clarify the metabolic characteristics of SNZ by gut microbiota, more intensive temporal sampling points were added. The second intestinal bacteria incubation system adopts the same system as the first one. The concentrations of SNZ were detected at 0, 0.25, 0.5, 1, 1.5, and 2 h after incubation. Fig. 1C shows that the concentration of SNZ decreased rapidly, and the original drug was metabolized by intestinal bacteria by 43.8%, 88.1%, and 100.0% at 15 min, 30 min, and 1 h, respectively.

To explore whether the liver exerts similar or other metabolic effects on SNZ, we incubated SNZ in liver homogenate or liver microsome system, respectively. In this study, the drug was incubated with the liver homogenate or liver microsomes for 0, 0.25, 0.5, 1, 1.5, and 2 h, and the content of the original drug in the samples was detected (Figs. 1D and E). After 2 h of interaction, SNZ in liver homogenate and liver microsomes did not change significantly, compared with the negative control group (only vehicle was added), indicating that neither liver homogenate nor liver microsomes exhibited significant metabolic effects on SNZ, and the liver is not the main vigorous metabolism site of SNZ.

To investigate the metabolites of SNZ produced by intestinal bacteria, we used HPLC-MS^n-IT-TOF to identify the suspected metabolites in the incubation system. As a result, two main potential metabolites (M1 and M2) were detected, of which retention times were 10.1 min and 11.3 min, respectively (Fig. 2A and Table 1). Fig. 2A shows the liquid chromatogram of the incubation system with a detection wavelength of 254 nm. The representative total ion chromatogram and extract ion chromatogram are shown in Fig. S1. Notably, the peaks of these metabolites were not detected in the inactivated negative control group, indicating that M1 and M2 were not substances produced by environmental effects, but by the metabolism of intestinal flora.

Based on high-resolution MS, we identified possible structures of the two metabolites. The mass spectrum of M1 along with the possible structure is shown in Figs. 2B and C. The molecular formula of M1 was $C_{14}H_{20}O_7$, and the molecular ion was displayed as $[M-H]^-$ ($C_{14}H_{19}O_7^-$) in MS and its *m/z* is 299.1160. Based on the high-resolution mass spectra obtained by TOF, we summarized the fragmentation progress as follows. The ion with *m/z* of 137.0616 is obtained by the loss of one glucose from the molecular ion ($[M-H-C_6H_{10}O_5]^-$, *m/z* 137.0616). The ion with *m/z* of 179.0545 is the glucose residue sourced from the molecular ion losing the aglycone ($[M-H-C_8H_8O]^-$, *m/z* 179.0545). The product ion with *m/z* 119.0356 is a glycosides-specific fragmentation ($[M-H-C_{10}H_{12}O_3]^-$, *m/z* 119.0356), which further removes a CH_2O to generate a product ion with *m/z* of 89.0252 ($[M-H-C_{10}H_{12}O_3-CH_2O]^-$, *m/z* 89.0252). Based on the molecular structure, molecular weight, and MS cleavage pathway of SNZ and M1, we speculate that M1 may be a metabolite after the hydrolysis from the carboxyl ester bond of SNZ. After comparison with the

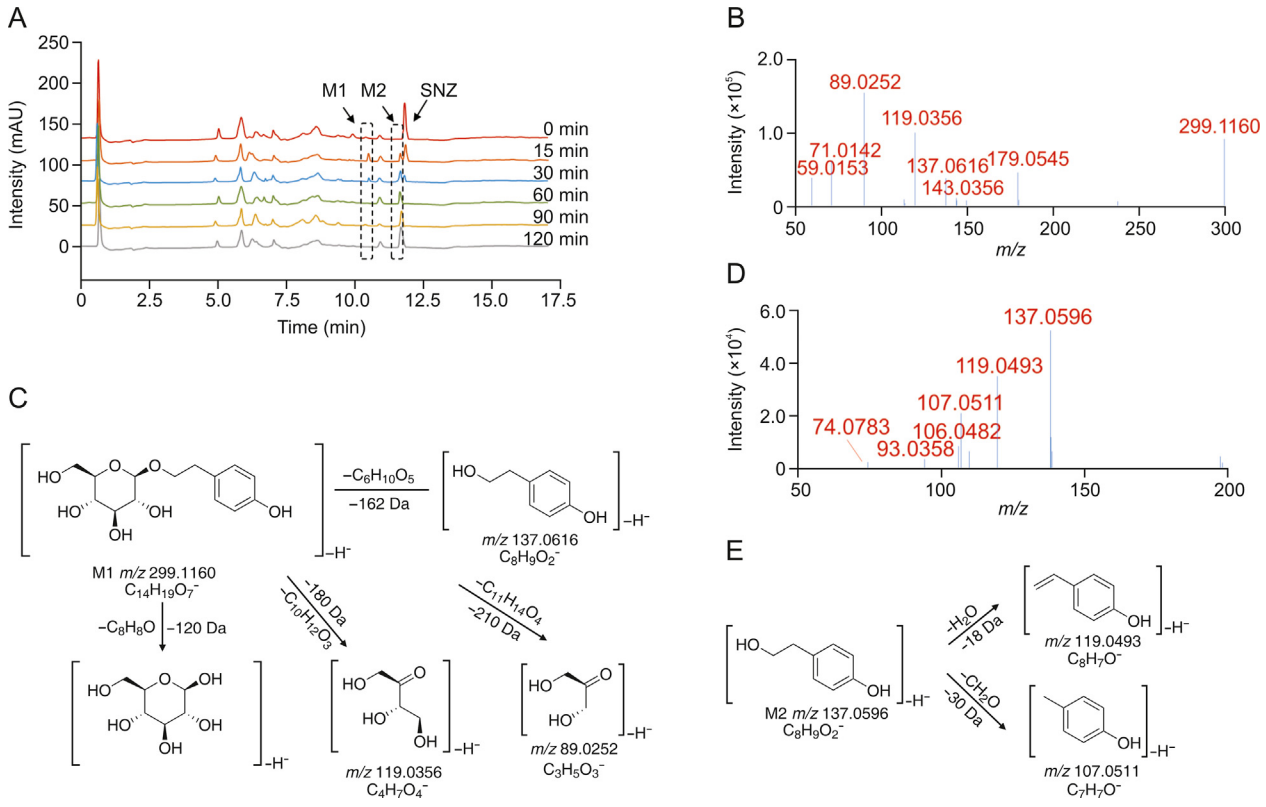

Fig. 2. Structural identification of specnuezhenide (SNZ) gut microbiota metabolites. (A) The liquid chromatogram of the intestinal bacteria incubation system with SNZ incubated for 2 h, and the detection wavelength was 254 nm. (B) The tandem mass spectrometry (MS/MS) data of the SNZ metabolite M1. (C) Possible structure and mass spectrometric cleavage pathway of metabolite M1. (D)The MS/MS data of the SNZ metabolite M2. (E) Possible structure and mass spectrometric cleavage pathway of metabolite M2.

Table 1
Characteristics of specnuezhenide (SNZ) metabolites in gut microbiota by high performance liquid chromatography coupled with an ion trap time-of-flight tandem mass spectrometry (HPLC/MS^n-IT-TOF).

Metabolites	Retention time (min)	Reaction	Predicted molecular weight	Molecular formula	Fragment characteristics	
					Mass spectrometry (MS; $[M-H]^-$)	MS/MS
M1	10.1	Hydrolysed	300.30	$C_{14}H_{20}O_7$	299.12	179.05, 137.06, 119.04, and 89.03
M2	11.3	Hydrolysed	138.16	$C_8H_{10}O_2$	137.06	119.05 and 107.05

standard substance, it was determined that M1 may be salidroside ($C_{14}H_{20}O_7$).

In addition, we found M2 with a smaller *m/z* ($[M-H]^-$, $C_8H_9O_2^-$) 137.0596 at a retention time of 11.3 min, and the molecular formula is $C_8H_{10}O_2$. The M2 mass spectrum and possible structure are shown in Figs. 2D and E. The high-resolution mass spectrum obtained from TOF as well as the mass fragmentation progress are summarized below. The ion with *m/z* of 119.0493 was obtained from the loss of one H_2O from the molecular ion ($[M-H-H_2O]^-$, *m/z* 119.0493). The molecular ion can also take off one CH_2O to generate the product ion with *m/z* 107.0511 ($[M-H-CH_2O]^-$, *m/z* 107.0511). Based on the molecular weight and the structure of SNZ, we believed that M2 may be the hydrolysis product of M1 by loss of glucose residue. After comparison with the standard substance, it was determined that M2 may be tyrosol ($C_8H_{10}O_2$).

Next, to clarify the metabolic characteristics of M1 and M2 by gut microbiota, a quantitative analysis method for detecting salidroside and tyrosol in intestinal bacterial matrix was established using HPLC-MS/MS. The chromatogram is shown in Fig. 3A. The retention time of salidroside in this method was 10.1 min, and the retention time of tyrosol was 11.3 min. After co-incubating the intestinal flora with SNZ for 0, 0.25, 0.5, 1, 1.5, and 2 h, 3-fold volume of methanol solution containing glipizide was added to the system to terminate the reaction. The production of potential metabolites was explored. As shown in Fig. 3B, salidroside was first rapidly generated in the system, and salidroside reached the highest peak (3.29 μg/mL) at 15 min. Then, the content of salidroside gradually decreased, indicating that salidroside is not the final product of intestinal bacterial metabolism. The content of tyrosol increased gradually with incubation time (Fig. 3C). The two metabolites were not detected in the inactivated control group, indicating that these two metabolites were produced by the metabolism of intestinal bacteria.

3.2. Pharmacokinetics of SNZ mediated by the gut microbiota

Since SNZ was metabolized by gut microbiota in vitro, it is necessary to investigate the effect of gut bacteria on the pharmacokinetic behavior of SNZ in mice. A PGF model was established 3 days after administration of erythromycin 200 mg/kg, oxytetracycline 200 mg/kg, and cefadroxil 100 mg/kg to healthy Balb/c mice. Fig. 3D shows the number of bacterial colony forming units (CFUs) in the intestinal contents of normal and PGF mice. The CFUs of the PGF group were significantly lower than those of the normal mice ($^{***}P < 0.001$) by 80.1%, which indicated that the gut microbiota was depleted under the action of antibiotics and that the PGF state was successfully established.

Then, SNZ (109.2 mg/kg) was orally administered to normal Balb/c mice and PGF mice. Figs. 3E–G demonstrate the time-concentration curves of SNZ, salidroside, and tyrosol, respectively.

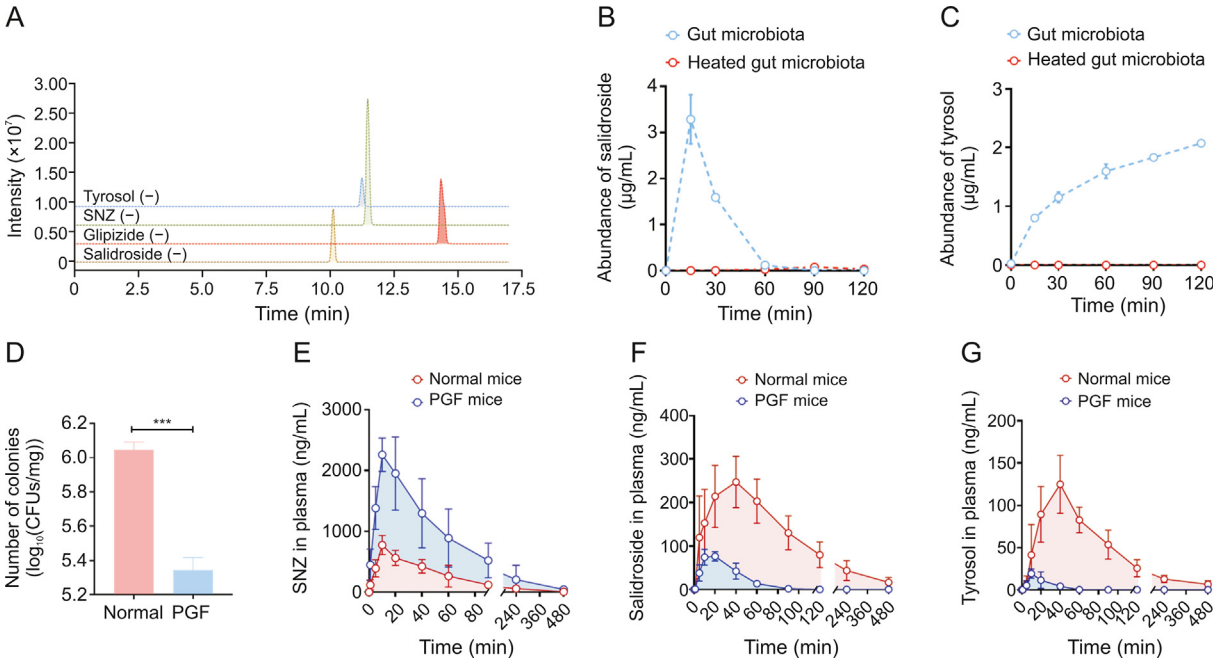

Fig. 3. Quantitative study of specnuezhenide (SNZ) intestinal bacteria metabolites and in vivo pharmacokinetic study. (A) Extract ion chromatogram of tyrosol, SNZ, glipizide, and salidroside. (B) Metabolic curve of salidroside in vitro. (C) Metabolic curve of tyrosol in vitro. (D) Number of colonies in intestinal contents of normal and pseudo-germfree (PGF) mice. (E) Pharmacokinetic time-concentration curve of SNZ in normal mice. (F) Pharmacokinetic time-concentration curve of salidroside in normal mice. (G) Pharmacokinetic time-concentration curve of tyrosol in normal mice. Data are presented as mean ± standard deviation. $^{***}P < 0.001$. CFUs: colony forming units.

Table 2
Pharmacokinetic parameters in normal Balb/c mice and pseudo-germfree (PGF) mice after oral administration of specnuezhenide (SNZ; 109.2 mg/kg).

Parameters	SNZ				Salidroside				Tyrosol	
	Normal		PGF		Normal		PGF		Normal	
	Mean	SD	Mean	SD	Mean	SD	Mean	SD	Mean	SD
$AUC_{(0-t)}$ (μg/L/min)	51191.08	16017.34	187946.85	68700.59	33814.78	6072.84	3079.01	859.31	13158.45	2024.93
$AUC_{(0-\infty)}$ (μg/L/min)	55211.00	19113.37	191167.49	70315.67	36004.16	7985.77	3205.99	801.92	13944.89	2151.59
$t_{1/2}$ (min)	110.14	68.39	82.57	31.67	90.82	51.44	14.24	2.42	110.25	33.82
t_{max} (min)	10.00	0.00	12.00	4.47	44.00	8.94	16.00	5.48	36.00	8.94
c_{max} (μg/L)	776.39	158.14	2310.30	289.72	257.29	44.59	82.70	8.34	125.80	32.73

SD: standard deviation; $AUC_{(0-t)}$: area under the curve (from zero to time of sample collection at which the last concentration can be accurately determined); $AUC_{(0-\infty)}$: area under the curve (from zero to infinity); $t_{1/2}$: half-life period; t_{max}: peak time; c_{max}: peak concentration.

The pharmacokinetic parameters are shown in Table 2. The peak concentration (c_{max}) and area under the curve (from zero to time of sample collection at which the last concentration can be accurately determined, $AUC_{(0-t)}$) of SNZ in the plasma of the PGF mice were 2.9 and 3.7 times higher than those of the normal mice, respectively, suggesting a weak metabolic activity in the gut under the PGF state (Fig. 3E and Table 2). Correspondingly, the exposure of salidroside and tyrosol to the PGF mice was also significantly lower than that of the normal mice (Figs. 3F and G and Table 2). In addition, the c_{max} and $AUC_{(0-t)}$ of salidroside in the normal mice were higher than those in the PGF mice (Fig. 3F and Table 2). Besides, the concentration of tyrosol in the PGF mice was lower than that in the normal group. However, the pharmacokinetic parameters could not be fitted due to the lack of detectable time points (Fig. 3G and Table 2). Based on this, we can speculate that the gut microbiota has an important effect on the pharmacokinetic characteristics of SNZ.

3.3. Carboxylesterase-mediated transformation of SNZ in the gut

SNZ contains carboxyl ester bonds, and the metabolites identified were the products of the hydrolysis of the ester bond. Therefore, we studied the role of carboxylesterases in bacterial flora on SNZ metabolism. First, the crystal structure of carboxylesterase (PDB 1AUO) was obtained from the PDB database, and then virtual molecular docking analysis was performed. Fig. 4A shows the virtual docking principle between SNZ and carboxylesterase. When SNZ was in contact with carboxylesterase, the two molecules exhibited strong docking ability with a binding free energy of −45.06 kcal/mol. Fig. 4B shows a two-dimensional schematic diagram of SNZ binding to carboxylate. As shown in Fig. 4B, there were many hydrophilic bonds (hydrogen bonds) in the active site of carboxylesterase, which may be the main binding force between SNZ and carboxylesterase. In addition, after the carboxylesterase inhibitor BNPP (0, 1, 5, and 10 mM) was added to the incubation

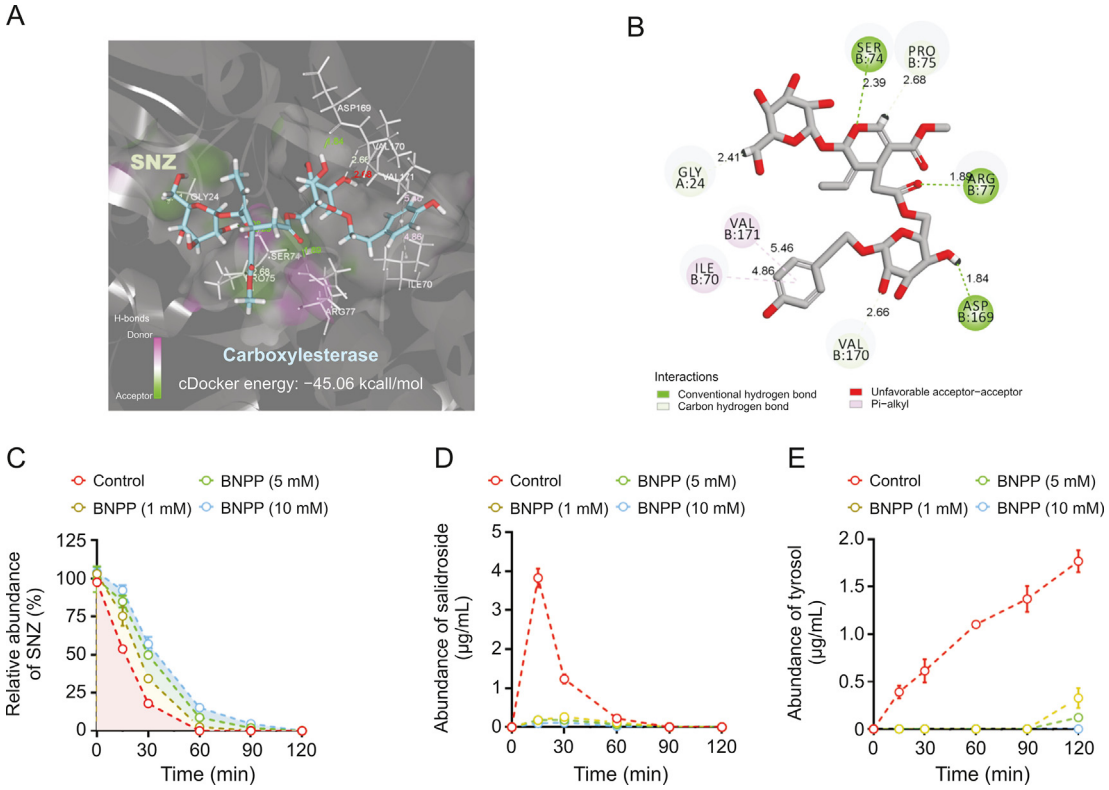

Fig. 4. Transformation of specnuezhenide (SNZ) to salidroside and tyrosol mediated by carboxylesterase. (A) Molecule docking principle between SNZ and carboxylesterase 1AUO. (B) 2D schematic diagram of the binding of SNZ to carboxylesterase. (C) Inhibition metabolic curve of SNZ by incubation with *bis-p*-nitrophenyl phosphate (BNPP) in vitro. (D) Inhibition of the conversion from SNZ to salidroside by incubation with BNPP in vitro. (E) Inhibition of the conversion from SNZ to tyrosol by incubation with BNPP in vitro.

system, the metabolic rate of SNZ was inhibited in a dose-dependent manner, which indicated that the carboxylesterase does take part in the metabolism of SNZ (Fig. 4C). Meanwhile, SNZ still can be completely consumed as the incubation time prolonged, which may be explained by the metabolism of glycosidic bonds on the SNZ by the gut microbiota. However, the corresponding structure was hardly detected, and we believe the sugar moiety was then rapidly transformed into other metabolites with smaller molecular weight, such as short chain fatty acids. Interestingly, the conversion of SNZ to salidroside and tyrosol, the metabolites from hydrolyzing the carboxyl ester bond, was significantly inhibited (Figs. 4D and E) after adding BNPP, and showed a dose-dependent manner. The contents of salidroside and tyrosol in BNPP groups were far lower than those in the control group. At 120 min, the inhibition rate of tyrosol production was 81.5%, 93.1%, and 100.0% as the concentration of BNPP increased, compared with the control group, respectively, which confirmed that generation of salidroside and tyrosol was dependent on the action of gut microbial carboxylesterase. Combined with the above results, the findings indicate that carboxylesterases of gut microbiota may be key bacterial enzymes for the conversion of SNZ to salidroside and tyrosol.

3.4. SNZ has antitumoral effect on tumor-bearing mice

Next, the pharmacological activity of SNZ was studied. An orthotopic colorectal tumor model was established. The experimental process is shown in Fig. 5A. Male Balb/c mice were injected into the anal epithelium with 2×10^6 murine colorectal tumor cells (colon 26 cells) to obtain a colorectal tumor model. The NPGF, the TPGF, and the SNZ TPGF group were given an oral gavage of cocktail antibiotics for three days after inoculation of cells to establish a PGF state. The results of the therapeutic effect of SNZ on colorectal tumors in mice are shown in Fig. 5. After 10 days of drug interventions, the body weight in the tumor group decreased ($^{*}P < 0.05$, Fig. 5B), while the body weight in the SNZ group was observed to increase slightly ($^{*}P < 0.05$, Fig. 5B). After collecting the tumor tissues, the size of the tumor tissues was measured. As shown in Fig. 5C, the tumor in the SNZ group was smaller than that in the tumor group, while the tumor size of the TPGF group and the SNZ TPGF group did not change significantly. The tumor weights were also measured. Compared with the tumor group, it was seen that the tumor weight decreased by 24.4% in the SNZ group ($^{**}P < 0.01$), while there was no significant difference between the TPGF group and the SNZ TPGF group compared with the model group, although the tumor weight of TPGF and SNZ TPGF was reduced to some extent (Fig. 5D). At the same time, the tumor ratio (ratio of tumor/body weight) was also compared, and it was found that the tumor ratio of the SNZ group decreased significantly by 30.8% ($^{***}P < 0.001$), while the TPGF group and the SNZ TPGF group both decreased slightly (Fig. 5E). Of note, the tumor weight ($^{*}P < 0.05$, Fig. 5D) and the tumor ratio ($^{*}P < 0.05$, Fig. 5E) of SNZ group were both lower than those of SNZ TPGF group, suggesting the gut microbiota takes part in the antitumoral activity of SNZ. Furthermore, it was observed that the weight of the spleen in the tumor group was increased ($^{*}P < 0.05$) compared with the normal group since the spleen weight is related to the inflammation and immunity homeostasis, while the weight of the spleen in SNZ group was recovered. Compared with the tumor group, the spleen weight decreased by 26.6% in SNZ group ($^{*}P < 0.05$), and the use of antibiotics neutralized the effect of SNZ and seemed to further aggravate lesions in the spleen (Fig. 5F). It was also observed that the spleen ratio (ratio of spleen/body weight) in the tumor group increased ($^{*}P < 0.05$) compared with the normal group, while decreased in SNZ group ($^{*}P < 0.05$) compared with the tumor group (Fig. 5G). The inflammatory factors including TNF-α, IL-6, and IL-1β in serum were detected to evaluate the whole-body inflammation progression. As shown in Figs. 5H–J, the TNF-α ($^{**}P < 0.01$), IL-6 ($^{*}P < 0.05$), and IL-1β ($^{*}P < 0.05$) levels in the tumor group were significantly higher compared with those in normal group. The TNF-α ($^{*}P < 0.05$), IL-6 ($^{*}P < 0.05$), and IL-1β ($^{*}P < 0.05$) contents of the SNZ group declined significantly, respectively, compared with those of the tumor group. The TNF-α, IL-6, and IL-1β contents of the TPGF and SNZ TPGF group were found to decrease due to their anti-inflammatory properties. The above results indicated that SNZ exhibited therapeutic effects on colorectal tumors, which was dependent on the intestinal flora.

3.5. SNZ intestinal bacterial metabolites can be distributed in various organs in tumor-bearing mice

The pharmacokinetic properties and tissue distribution of SNZ in colorectal tumor mice was investigated to further understand the potential therapeutic mechanism of SNZ. Colorectal tumor mice and PGF tumor mice were orally fed with SNZ (109.2 mg/kg). Figs. 6A–C show the time-concentration curves of SNZ, salidroside, and tyrosol in tumor mice. Meanwhile, the pharmacokinetic parameters were shown in Table 3. The c_{max} and $AUC_{(0-t)}$ of SNZ in the plasma of PGF tumor mice were 2.7 and 4.9 times higher than those in the plasma of the tumor mice, respectively (Fig. 6A and Table 3). Meanwhile, the plasma exposures in salidroside and tyrosol in the PGF tumor mice were significantly lower than those in the tumor mice (Figs. 6B and C and Table 3). In addition, the c_{max} and $AUC_{(0-t)}$ of salidroside in the plasma of the tumor mice were higher than those in the plasma of the PGF tumor mice, respectively (Fig. 6B and Table 3). The exposure of tyrosol in the plasma in the tumor mice was significantly higher than that in PGF tumor mice. Due to fewer detectable time points, so the pharmacokinetic parameters of tyrosol could not be fitted (Fig. 6C and Table 3).

At the same time, the tissue distribution of SNZ was investigated, and it was found that the intestinal bacterial metabolites salidroside and tyrosol of SNZ could be distributed in various tissues (Figs. 6D and E). Salidroside can be distributed in liver, kidney, stomach, small intestine, etc., while tyrosol can be distributed in the liver, kidney, stomach, small intestine, heart, spleen, lung, colon, and other organs and tissues. It was worth noting that after oral administration of SNZ (109.2 mg/kg) for 20 min, a large amount of salidroside ($^{**}P < 0.01$) and tyrosol ($^{***}P < 0.001$) were detected in tumor tissue of tumor mice compared with PGF tumor mice (Figs. 6F and G). This result indicated that SNZ gut bacteria metabolites salidroside and tyrosol can directly interact with the tumor and may be the effective substances of anticancer effect of SNZ.

3.6. SNZ induced the production of short-chain fatty acids in vitro and in vivo

Short-chain fatty acid has been reported to play a role in reducing inflammation [41]. Especially, the butyric acid exhibited the antitumor activity and increase the efficacy of anticancer therapy [42]. Thus, the content of short-chain fatty acids in the incubation system was measured to investigate whether the SNZ could influence the function of gut microbiota. As shown in Figs. 7A–C, compared with the control group, SNZ could significantly promote and stimulate the intestinal flora to produce short-chain fatty acids, including butyric acid (Fig. 7A, $^{***}P < 0.001$), propionic acid (Fig. 7B, $^{***}P < 0.001$), and acetic acid (Fig. 7C, $^{***}P < 0.001$). At the same time, the animal feces of each group were collected, and then the content of short-chain fatty acids in the animal feces was detected. As shown in Figs. 7D–F, compared with the normal group, the content of short-chain fatty acids in the fecal samples of the tumor group decreased, including butyric acid (Fig. 7D, $^{*}P < 0.05$),

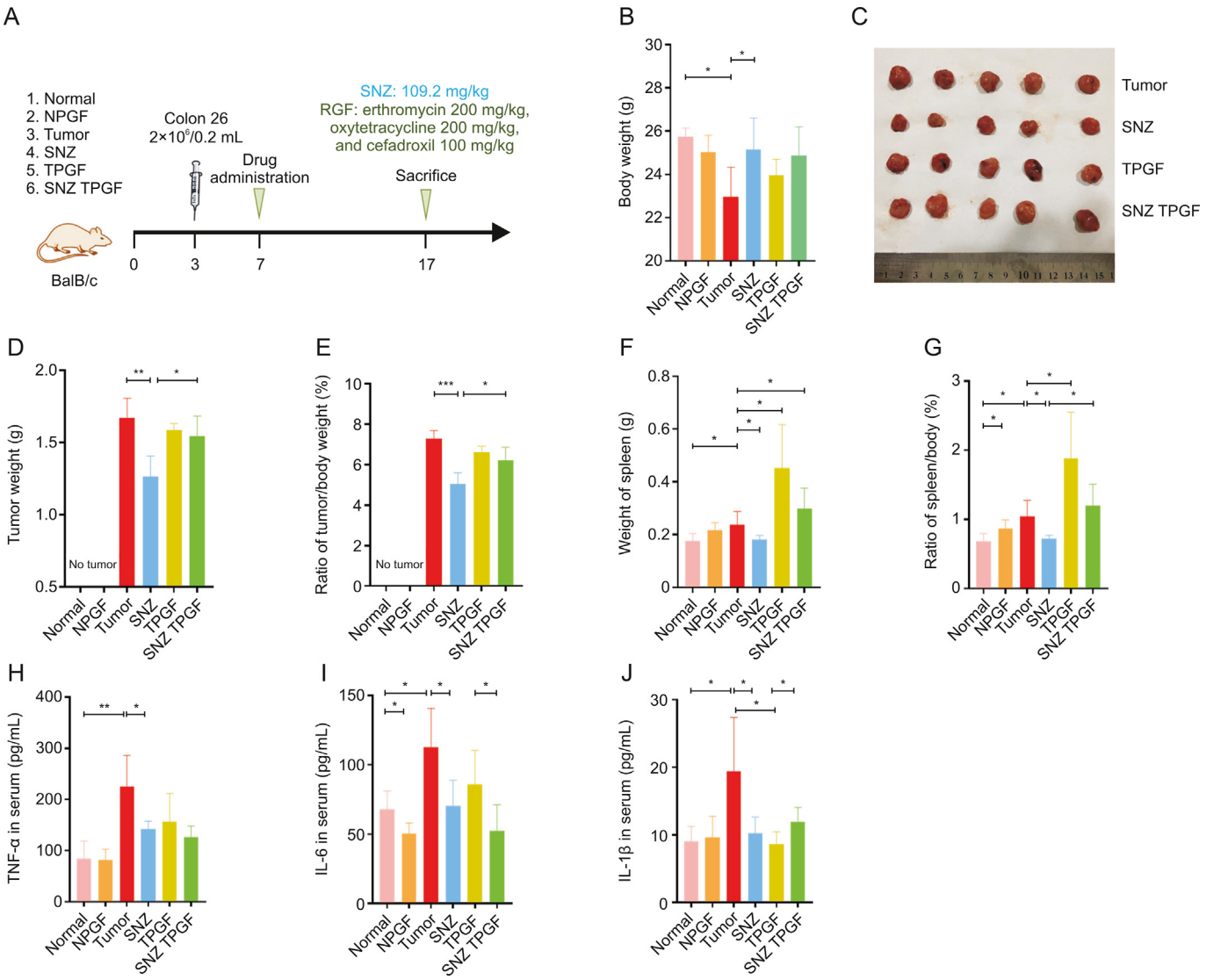

Fig. 5. The antitumoral activity of specnuezhenide (SNZ). (A) Experiment scheme of pharmacological effect of SNZ. (B) Animal weight after 10 days of treatment. (C) Tumors were harvested and taken pictures by a digital camera. (D) Tumor weight in each group. (E) Ratio of tumor weight/body weight in each group. (F) Spleen weight in each group. (G) Ratio of spleen weight/body weight in each group. (H) Tumor necrosis factor-α (TNF-α), (I) interleukin-6 (IL-6), and (J) IL-1β in serum. Data are presented as mean ± standard deviation. $^{*}P < 0.05$, $^{**}P < 0.01$, and $^{***}P < 0.001$. NPGF: normal pseudo-germfree (PGF) group; TPGF: PGF tumor group; SNZ TPGF: PGF tumor and SNZ group.

propionic acid (Fig. 7E, $^{*}P < 0.05$), and acetic acid (Fig. 7F, $^{**}P < 0.01$), suggesting that the intestinal flora in the tumor group has been disturbed. Meanwhile, we found that SNZ group promoted the production of short-chain fatty acids in tumor-bearing mice, such as butyric acid was up-regulated by 38.3% compared with the tumor group (Fig. 7D, $^{**}P < 0.01$), while the content of propionic acid was up-regulated by 30.8% compared with the tumor group (Fig. 7E, $^{**}P < 0.01$), and the acetic acid by 38.9% compared with the tumor group (Fig. 7F, $^{**}P < 0.01$). In addition, it was also observed that the use of antibiotics substantially eliminated short-chain fatty acids in the feces of each group. Thus, we can infer that SNZ stimulated the production of short-chain fatty acids both in vitro and in vivo.

3.7. SNZ regulated the composition of the intestinal microbiota and gut mycobiota

Then, we investigated whether SNZ influence the composition of gut microbiome. After 10 days of oral administration of SNZ, fecal samples were collected for analysis of gut microbiota composition. The differences in gut microbiota were investigated by 16S rRNA gene sequencing and pyrosequencing of the V3 and V4 regions. Fig. 8A shows the α-diversity of the fecal sample in each group. α-diversity indicated the number of microbial species in a single sample and the proportion of each species. The Chao1 index and Shannon index of the NPGF group, the TPGF group, and the SNZ TPGF group were significantly decreased, compared with the normal group. The α-diversity in the tumor group showed a downward trend, while the Chao1 index and Shannon index of the intestinal flora recovered in SNZ group. Fig. 8B shows the β-diversity of the fecal sample flora which illustrates the similarities and differences among samples. The tumor group deviated from the Normal group, suggesting the intestinal flora was greatly changed under the tumor conditions, while the SNZ group situated close to the normal group, which indicated SNZ restored the disturbance of intestinal flora under the tumor state to a certain extent. Fig. 8C shows the distribution at the phylum level of the microbiota. Compared with the normal group, the proportion of

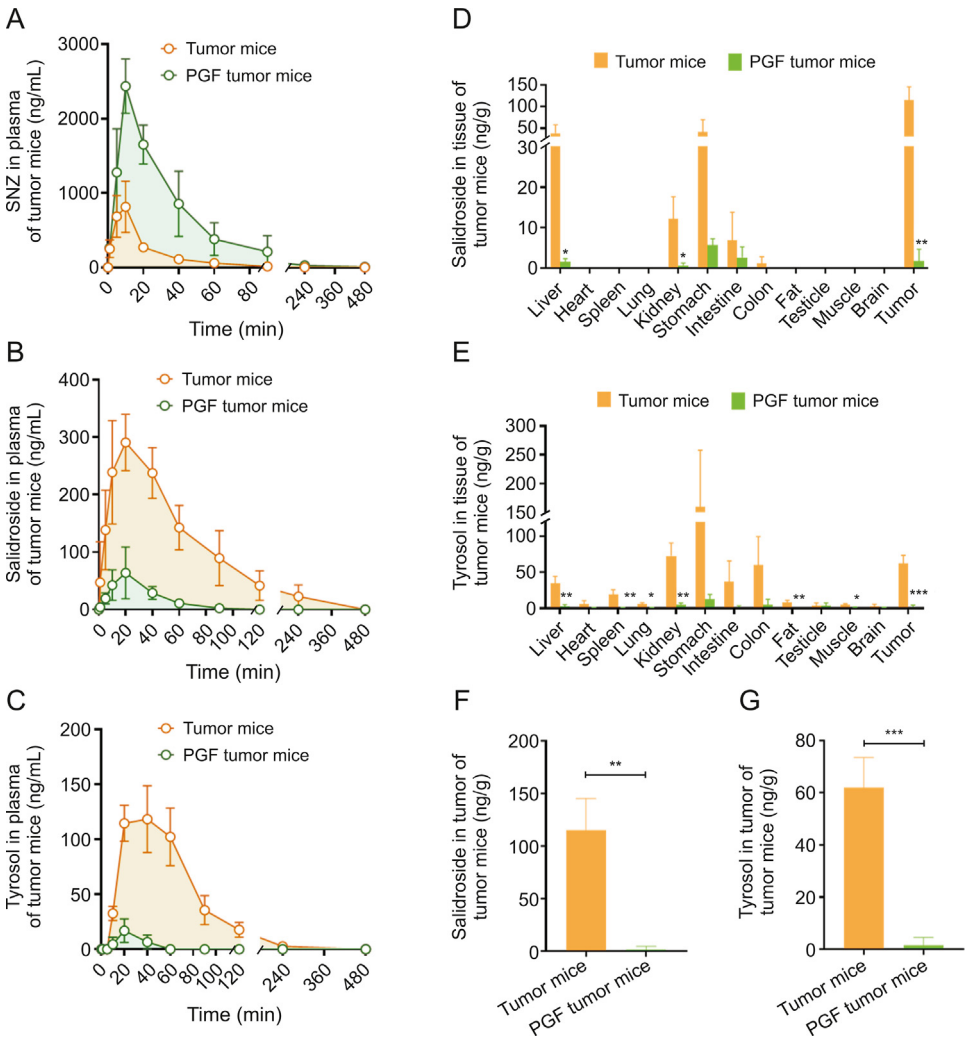

Fig. 6. Pharmacokinetic study of specnuezhenide (SNZ) in tumor mice. (A) The pharmacokinetic time-concentration curve of SNZ in tumor mice. (B) Pharmacokinetic time-concentration curve of salidroside in tumor mice. (C) Pharmacokinetic time-concentration curve tyrosol in tumor mice. (D) Tissue distribution of salidroside in tumor mice. (E) Tissue distribution of tyrosol in tumor mice. (F) Concentration of salidroside in tumor site. (G) Concentration of tyrosol in tumor site. Data are presented as mean ± standard deviation. $^{**}P < 0.01$ and $^{***}P < 0.001$. PGF: pseudo-germfree.

Table 3
Pharmacokinetic parameters in tumor mice and pseudo-germfree (PGF) tumor mice after oral administration of specnuezhenide (SNZ; 109.2 mg/kg).

Parameters	SNZ				Salidroside				Tyrosol	
	Normal		PGF		Normal		PGF		Normal	
	Mean	SD	Mean	SD	Mean	SD	Mean	SD	Mean	SD
$AUC_{(0-t)}$ (μg/L/min)	18752.02	3627.44	93688.66	29997.30	22373.93	5714.01	2207.64	889.49	8918.61	1333.62
$AUC_{(0-\infty)}$ (μg/L/min)	18817.56	3656.74	94414.35	30656.63	23773.54	5179.09	2452.12	1107.57	9833.89	1386.34
$t_{1/2}$ (min)	27.09	10.41	65.50	34.44	43.89	13.61	20.36	7.23	39.59	14.47
t_{max} (min)	8.00	2.74	10.00	0.00	18.00	4.47	18.00	4.47	32.00	17.89
c_{max} (μg/L)	919.22	268.35	2435.66	365.18	292.08	50.33	74.99	35.39	134.49	15.24

SD: standard deviation; $AUC_{(0-t)}$: area under the curve (from zero to time of sample collection at which the last concentration can be accurately determined); $AUC_{(0-\infty)}$: area under the curve (from zero to infinity); $t_{1/2}$: half-life period; t_{max}: peak time; c_{max}: peak concentration.

Bacteroidetes decreased significantly in the tumor group, while the proportion of *Proteobacteria* increased, and *Firmicutes*/*Bacteroidetes* (F/B%) increased, which was a biomarker for evaluating the pathological state and the lower F/B% correlated with a healthier state. After treatment with SNZ, the F/B% decreased significantly. We further analyzed the composition of intestinal flora at the genus level in the normal group, tumor group, and SNZ group. As shown in Fig. 8D, in the heatmap of top 30 genera, *Alistipes*, *Lachnospiraceae_UCG-001*, *Lachnospiraceae_NK4A136_group*, *Prevotellaceae_UCG-001*, *Bilophila*, *Parabacteroides*, *Helicobacter*, *Clostridium_sensu_stricto_1* increased in abundance in model group, while *Anaerotruncus*, *Butyicicoccus*, *Lactobacillus*, and *Rikenellaceae_RC9_gut_group* decreased in abundance. In addition, the abundance of some genera, such as *Anaerotruncus*, *Butyricicoccus*, *Lactobacillus*, *Rikenellaceae_RC9_gut_group*, etc., increased in the SNZ group compared with the tumor group, while *Roseburia*,

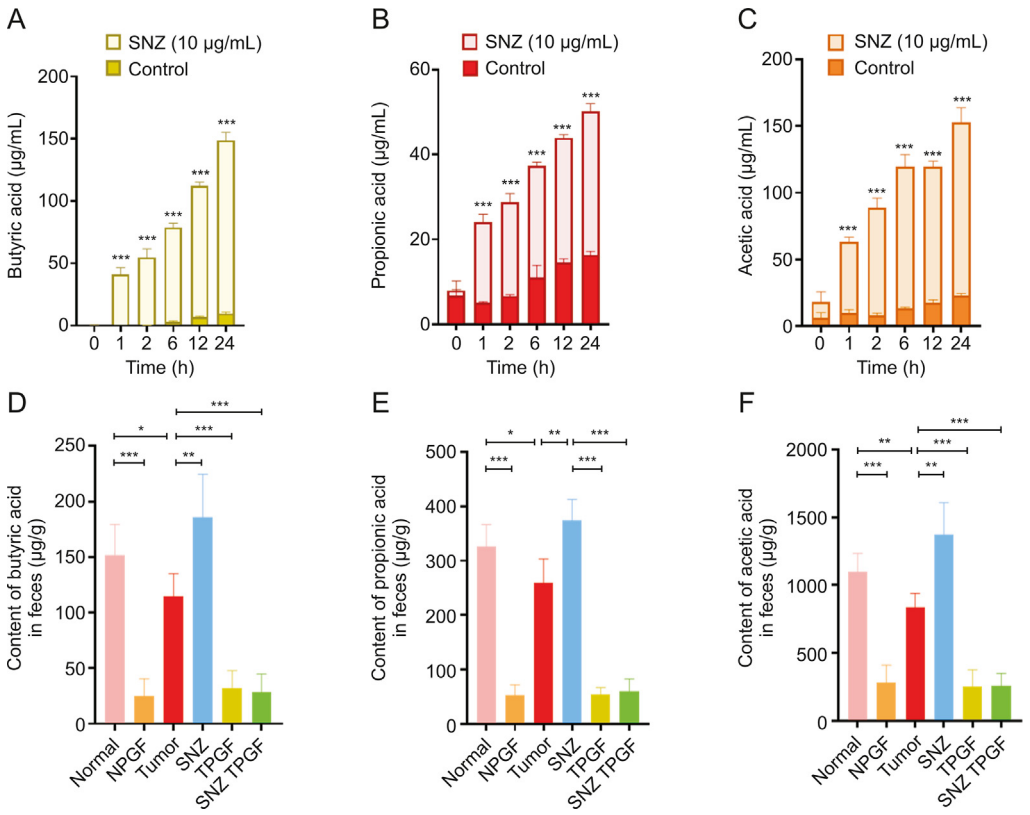

Fig. 7. Specnuezhenide (SNZ) stimulated gut microbiota to produce short-chain fatty acids in vivo and in vitro. (A) Butyric acid content in the co-incubation system of intestinal bacteria and SNZ in vitro. (B) Propionic acid content in the co-incubation system of intestinal bacteria and SNZ in vitro. (C) Acetic acid content in the co-incubation system of intestinal bacteria and SNZ in vitro. (D) Butyric acid content in feces of animals in vivo. (E) Propionic acid content in feces of animals in vivo. (F) Acetic acid in feces of animals in vivo. Data are presented as mean ± standard deviation. $^{*}P < 0.05$, $^{**}P < 0.01$, and $^{***}P < 0.001$. NPGF: normal pseudo-germfree (PGF) group; TPGF: PGF tumor group; SNZ TPGF: PGF tumor and SNZ group.

Lachnospiraceae_UCG-001, *Lachnospiraceae_NK4A136_group*, *Enterorhabdus*, *Desulfovibrio*, *Bilophila*, *Parabacteroides*, *Helicobacter*, and *Clostridium_sensu_stricto_1* decreased. Fig. 8E demonstrates the representative genera with significant changes between tumor group and normal group. *Lachnospiraceae UCG*-001 has been reported to be more abundant in older female mice than in younger females, suggesting that it is associated with aging [43]. *Prevotellaceae_UCG-001* is associated with the pathogenesis of colitis [44]. Stomach infection caused by *Helicobacter pylori* in *Helicobacter* is reported to be associated with progression of distal gastric cancer and gastric mucosal lymphoma in humans [45]. *Anaerotruncus* is associated with protection from hepatocellular carcinoma [46]. *Clostridium perfringens* was reported to be associated with colorectal cancer in an elderly woman [47]. *Butyricicoccus* produces butyrate and simultaneously modulates short-chain fatty acid transporters and receptors to inhibit 1,2-dimethylhydrazine-associated colorectal cancer progression [48]. *Lactobacillus*, a common probiotic, has been reported to provide anticancer effects by promoting tumor cell apoptosis and reducing oxidative stress, while also reducing the abundance of the cancer-promoting microorganism *Fusobacterium* [49].

In addition, we also analyzed the composition of mycobiota in normal group, tumor group, and SNZ group. As shown in Fig. 9, the Shannon index and Chao1 index in tumor group showed an upward trend, but a downward trend in SNZ group (Figs. 9A and B). Fig. 9C shows the β-diversity in each group. The SNZ group situated closer to normal group than tumor group, suggesting the abnormal composition of tumor group occurred and the SNZ showed the ability to restore this abnormality. By analyzing the characteristics of the mycobiota at the phylum level, it was found that the relative abundance of *Basidiomycota* and *Ascomycota* increased in the tumor group, but decreased in the SNZ group (Fig. 9D). Intestinal fungi tend to metabolize and grow more vigorously under the pathological conditions. Further analysis of the characteristics at the genus level was shown in Fig. 9E. The relative abundance of several genera, including *Aspergillus* and *Acremonium*, increased in tumor group compared with normal group, but decreased in the SNZ group (Fig. 9F). In addition, the relative abundances of *Candida* and *Penicillium* decreased in tumor group and gradually recovered in SNZ group (Fig. 9F). It has been reported that *Candida* contains a variety of human commensal species, such as *Candida albicans*, which can alleviate the intestinal mucosal damage caused by dextran sulfate-induced colitis in mice, exhibit immunomodulatory properties, and maintain intestinal homeostasis [50]. *Penicillium* has been reported to produce multiple secondary metabolites that inhibit tumor cell growth [51]. *Aspergillus* produces aflatoxins, which can cause opportunistic infections and liver damage in humans [52], and recent studies have shown that its abundance is increased in the gut of patients with multiple sclerosis [53]. *Acremonium* is an opportunistically pathogenic fungus that may invade the host in disease states and aggravate host infection [54].

Finally, since the SNZ showed a unique ability to change microbial spectrum and exhibited an anticancer effect, it is necessary to elucidate the relationship between the gut microbiome and the tumor-related factors and the role of SNZ in the treatment of colon cancer. We performed a correlation analysis of the detected tumor-related indices with the gut microbiome (Fig. 9G). It was observed that *Lactobacillus*, *Candida*, and *Anaerotruncus* were negatively

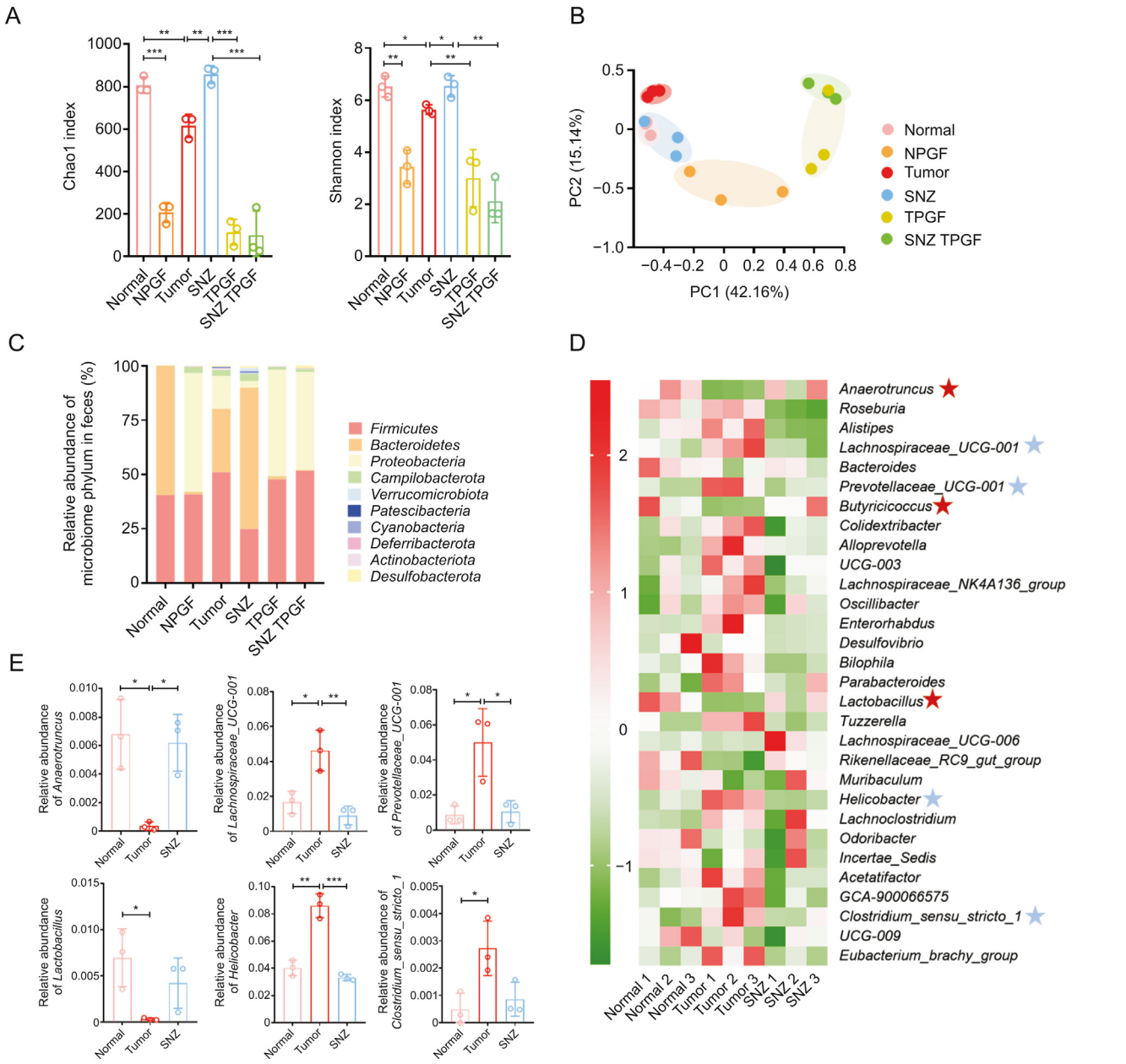

Fig. 8. Specnuezhenide (SNZ) modulated gut microbiota composition in tumor mice. (A) Chao1 index and Shannon index of gut bacteria. (B) β-diversity of gut bacteria. (C) The distribution of intestinal bacteria at phylum level. (D) Top 30 heat map of intestinal bacteria at genus level (blue star: the genus shows downtrends in SNZ group; red stars: the genus shows uptrends in SNZ group). (E) The representative genus with significant changes between tumor group and normal group. Data are presented as mean ± standard deviation. $^{*}P < 0.05$, $^{**}P < 0.01$, and $^{***}P < 0.001$. NPGF: normal pseudo-germfree (PGF) group; TPGF: PGF tumor group; SNZ TPGF: PGF tumor and SNZ group; PC: principal component.

correlated with tumor ratio and tumor weight, and *Prevotellaceae_UCG-001*, *Clostridium_sensu_stricto_1*, and *Aspergillus* were negatively correlated with tumor ration and tumor weight. Moreover, *Lactobacillus* and *Candida* were related to lower inflammatory factors and relieved spleen swelling, and *Lachnospiraceae_UCG-001*, *Helicobacter*, *Aspergillus* and *Acremonium* seemed to be responsible for the inflammation. In addition, *Prevotellaceae_UCG-001*, *Lachnospiraceae_UCG-001*, *Helicobacter*, and *Acremonium* were negatively related to the content of short-chain fatty acids in feces. *Lactobacillus* and *Anaerotruncus* tended to be related to an increased content of short-chain fatty acids.

4. Discussion

FLL is a traditional Chinese medicinal that nourishes the liver and kidneys and improves eyesight and hair. It exhibits a wide range of pharmacological effects, such as anti-inflammatory and analgesic, immune regulation, and antibacterial and antiviral effects. Currently, FLL is used in various Chinese patent preparations, including Erzhi Pills. As the main component of FLL and Chinese patent preparations containing FLL, SNZ exhibits pharmacological activities such as anti-inflammatory [11], antioxidative stress [14], and pancreatic islet protection [12]. Our study showed that SNZ

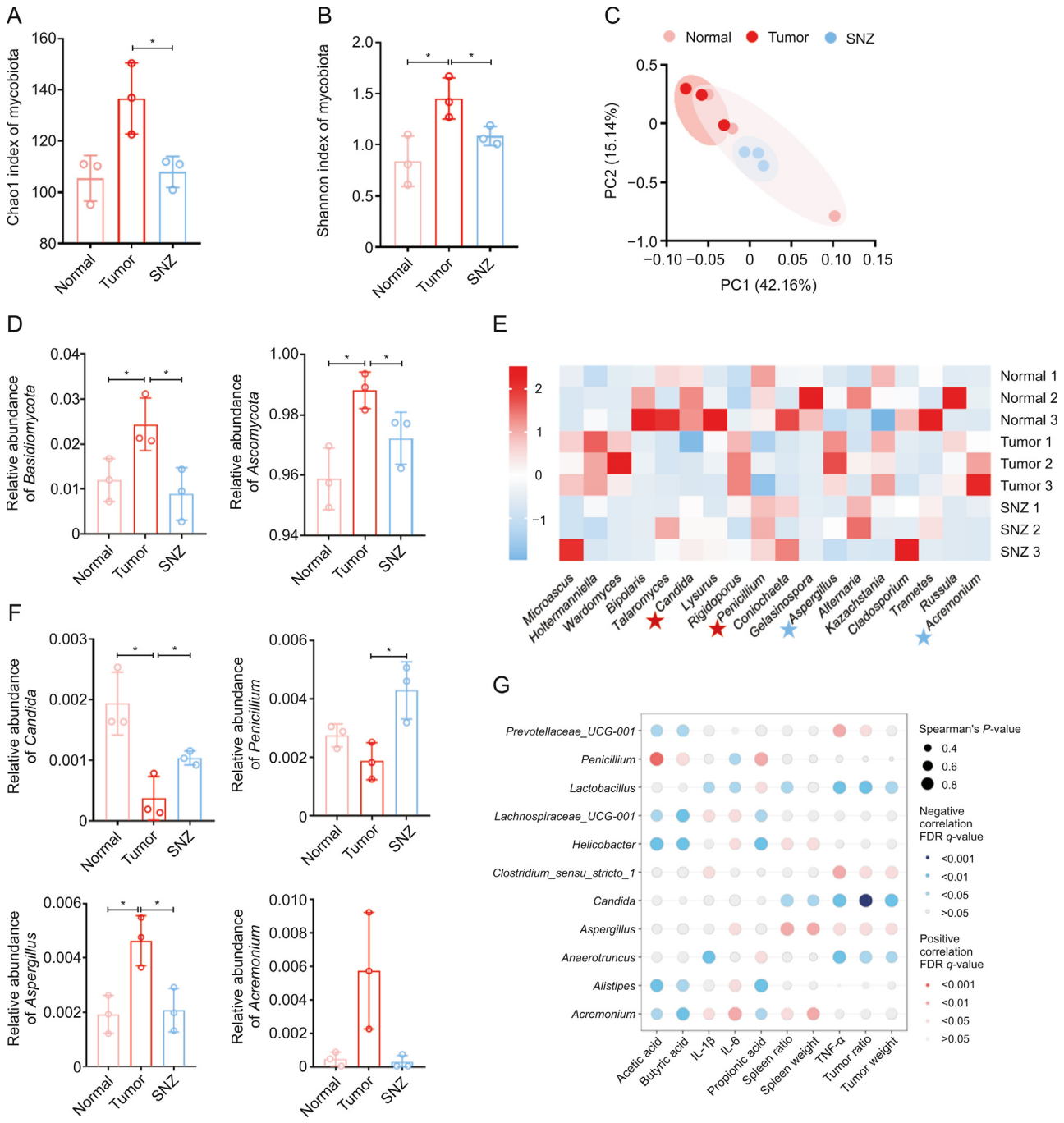

Fig. 9. Specnuezhenide (SNZ) modulates gut mycobiota composition in tumor mice. (A) Chao1 index of gut fungi. (B) Shannon index of gut fungi. (C) β-diversity of gut fungi. (D) Relative abundance of *Basidiomycota* and *Ascomycota* in each group. (E) Top 18 heat map of the gut mycobiota in genus level (blue star: the genus shows downtrends in SNZ group; red stars: the genus shows uptrends in SNZ group). (F) The representative fungi genus with significant changes among groups. (G) Correlation analysis between tumor-related factors and gut microbiome at the genus level. Data are presented as mean ± standard deviation. $^{*}P < 0.05$. IL: interleukin; TNF: tumor necrosis factor; FDR: false discovery rate.

could inhibit tumor development in a mouse colorectal tumor model to some extent.

However, SNZ belongs to iridoid glycosides, which exhibit poor oral bioavailability; therefore, its pharmacological activity should be closely related to its metabolism in vivo. In this study, we discovered the unique metabolic effects of SNZ by gut microbes. We mainly found and confirmed two possible stable metabolites of SNZ from gut bacteria. After molecular weight comparison, it was determined the metabolites may be the hydrolysis products of the ester bond on SNZ. The molecular formulas are: $C_{14}H_{20}O_7$ ($[M-H]^-$, *m/z* 299.1160, M1) and $C_8H_{10}O_2$ ($[M-H]^-$, *m/z* 137.0596, M2). Then, the structures and MS fragmentation pathways were analyzed by HPLC-MS^n-IT-TOF. Compared with the standard substances, the two metabolites were identified as salidroside and tyrosol, of which salidroside is the metabolite after hydrolyzing the carboxylic ester bond on SNZ, and tyrosol is the aglycone of salidroside. However, in vitro liver homogenate metabolism experiments and liver microsome experiments showed that the metabolism ability of SNZ

by the liver was very weak.

It was worth noting that salidroside and tyrosol were detected in the plasma of mice after oral administration of SNZ. Compared with the pharmacokinetics study of SNZ in normal mice, the levels of salidroside and tyrosol in the plasma of PGF mice were significantly lower, while the exposure of SNZ in the plasma of mice in the PGF mice was increased. It was suggested that the reduced abundance of gut microbiota due to antibiotics impairs its hydrolysis of SNZ, which can promote the absorption of SNZ and reduce the biotransformation of SNZ to salidroside and tyrosol. The above-mentioned factors may explain the low bioavailability of SNZ after oral administration. The tissue distribution study in colorectal tumor mice showed that salidroside and tyrosol can be distributed in various organs. After using antibiotics to deprive the metabolism of microbial enzymes in the gut, the concentrations of salidroside and tyrosol in tissues of PGF tumor mice were significantly reduced. It was worth noting that both salidroside and tyrosol can be distributed in the tumor sites, suggesting that intestinal bacterial metabolites of SNZ may be the effective substances with antitumor effects. These two possible metabolites may possess multiple pharmacological activities. For example, salidroside has been reported to have anticancer effects by promoting apoptosis and protective autophagy in human adeno gastro carcinoma cells induced by the phosphatidylinositol 3-kinase/protein kinase B/mammalian target of rapamycin pathway [55]. In addition, salidroside also provides therapeutic effects on poorly differentiated thyroid cancer and liver cancer through various mechanisms [56,57]. At the same time, salidroside has antioxidative stress, anti-aging, and anti-inflammatory effects, and has significant activity on the cardiovascular system and central nervous system [58]. Tyrosol is the aglycone of salidroside, which shows biological activities such as antioxidant, stress protection, anti-inflammatory, anti-cancer, cardioprotection, neuroprotection, etc.. Tyrosol has emerged as a promising neuroprotective agent for ischemic stroke [59]. It was reported that tyrosol will continue to metabolized into tyrosol sulfate once absorbed into the body, which has the potential of anti-oxidant and anti-inflammation effects [60]. These results further demonstrated that the gut microbial metabolites of SNZ may enter the tumor site to exert antitumor effects.

Next, we investigated which factors mediated this biotransformation (from SNZ to salidroside/tyrosol). Through virtual molecular docking study and inhibitor experiments, we found that carboxylesterase is one of the key enzymes mediating this transformation process. The inhibitor experiment showed that the carboxylesterase inhibitor BNPP significantly delayed the metabolic rate of SNZ within 120 min (high concentration of BNPP (10 mM) can prolong approximately 60 min compared with the control group). Salidroside and tyrosol were significantly inhibited by BNPP. Although SNZ was completely metabolized within 120 min in the incubation system with the existence of BNPP, this may be due to the fact that the sugar residue in the SNZ may act as the dominant carbon source of the gut microbiota. The preferential uptake of the sugar moiety led to other biotransformations of SNZ [54], and the intermediate metabolites produced were likely to be unstable and therefore not significantly detected in our study. Interestingly, carboxylesterases played an important role in the transformation process, and the interaction of SNZ with gut bacteria was similar to that of albiflorin in our previous work [61]. In addition, a virtual molecular docking study confirmed that the isoform of carboxylesterase that mediates the biotransformation of SNZ may be carboxylesterase 1AUO.

Furthermore, microbial diversity analysis showed that SNZ could alleviate tumor progression by modulating the abundance of intestinal flora and increasing the abundance of probiotics. We found that the abundance of *Lactobacillus* was increased in the SNZ-treated animals. By referencing the database, the *Lactobacillus* genus was reported to contain a large number of gene fragments encoding enzymes with similar functions to carboxylesterases, which was consistent with the previous results [62]. It was suggested that the interaction of SNZ with gut microbiota further promoted the therapeutic effect of SNZ.

In addition, since salidroside and tyrosol are polyphenolic compounds, it has been reported salidroside and tyrosol also have the ability to modulate the structure of the gut microbiota [63]. In addition, SNZ also regulated the abundance of some short-chain fatty acid-producing genera, such as *Butyricicoccus* [48], *Lactobacillus* [64], *Anaerotruncus* [65], etc., thereby increasing the content of short-chain fatty acids in feces, which also corresponded to the results of in vitro incubation experiment. Intestinal bacteria can use SNZ as the sole carbon source, and the glycosyl moiety of SNZ was eventually metabolized into short-chain fatty acids by intestinal bacteria. On the other hand, polyphenol metabolites such as

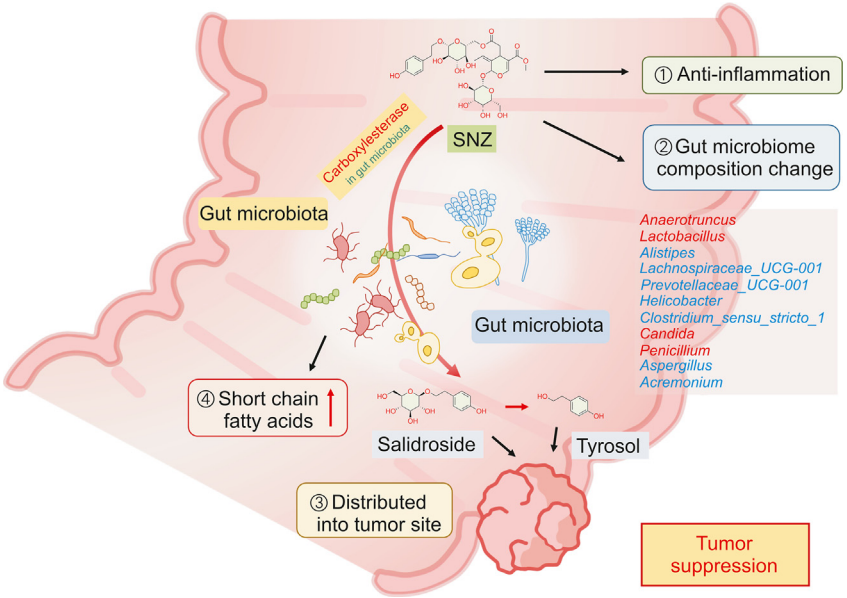

Fig. 10. The metabolic pathway of specnuezhenide (SNZ) by gut microbiota and possible tumor-suppression therapeutic mechanism of SNZ.

salidroside and tyrosol can be further converted into short-chain fatty acids by gut microbes [66]. Short-chain fatty acids have been reported to prevent colitis by modulating immunity and stabilizing intestinal regulatory T cells [67], which may correspond to the remission of the pathological condition of the splenomegaly in mice given SNZ. Intestinal fungi also changed to a certain extent in this study, which may be the direct effect of SNZ on the fungal group, since polyphenols have been reported to kill some pathogenic fungi [68]. The changes in gut mycobiota may also be a secondary response to the balance disturbance of the intestinal flora, which echoes the previous conclusions [69–71]. The metabolic pathway by gut microbiota and possible tumor-suppression therapeutic mechanism of SNZ are shown in Fig. 10.

5. Conclusion

In this study, the interaction between SNZ, the main component of the traditional Chinese medicine FLL, and the intestinal microbes was explored. The carboxylesterase in intestinal microbiota was one of the main enzymes involved in the metabolism of the SNZ. In addition, we identified salidroside and tyrosol as the gut microbiota metabolites of SNZ. SNZ can also stimulate the secretion of short-chain fatty acids by intestinal flora in vitro and in vivo and showed anti-inflammatory effects in vivo. Oral administration of SNZ to colorectal tumor mice showed that SNZ had the potential to inhibit tumor growth, and this effect was dependent on the intestinal microbes. Moreover, the gut microbiota-based pharmacokinetics characteristics of SNZ as well as the two metabolites in mice suggested the salidroside and tyrosol may be the therapeutic substances of SNZ to suppress tumor growth, since salidroside and tyrosol can be distributed in tumor site. Furthermore, SNZ can also regulate the composition of the gut microbiota and gut mycobiota, which may contribute to the efficacy of SNZ.

CRediT author statement

Hang Yu: Writing - Original draft preparation, Reviewing and Editing; **Hui Xu:** Writing - Reviewing and Editing; **Xinyu Yang:** Investigation, Validation; **Zhengwei Zhang**, **Jiachun Hu**, and **Jinyue Lu:** Validation; **Jie Fu** and **Mengmeng Bu:** Investigation; **Haojian Zhang**, **Zhao Zhai**, and **Jingyue Wang:** Validation; **Jiandong Jiang:** Conceptualization, Methodology, Supervision; **Yan Wang:** Conceptualization, Methodology, Writing - Original draft preparation, Reviewing and Editing.

Declaration of competing interest

The authors declare that there are no conflicts of interest.

Acknowledgments

This project was supported by the National Key R&D Program of China (Grant No.: 2022YFA0806400), the CAMS Innovation Fund for Medical Sciences (Grant Nos.: 2022-I2M-1-028, 2022-I2M-2-002, and 2021-I2M-1-007), the National Natural Science Foundation of China (Grant Nos.: 81973290 and 82173888), and Beijing Key Laboratory of Non-Clinical Drug Metabolism and PK/PD study, China (Grant No.: Z141102004414062). We would like to thank Shimadzu (China) Co., Ltd. for technological support.

Appendix A. Supplementary data

Supplementary data to this article can be found online at https://doi.org/10.1016/j.jpha.2023.06.012.

References

[1] Z.T. Pang, Z.Y. Zhou, W. Wang, et al., The advances in research on the pharmacological effects of Fructus Ligustri Lucidi, BioMed Res. Int. 2015 (2015), 281873.
[2] X. Ji, X.-Q. Liu, L. Gao, et al., Qualitative and quantitative analysis on triterpenoids in *Ligustri Lucidi Fructus*, Zhongguo Zhong Yao Za Zhi 46 (2021) 1168–1178.
[3] L. Gao, C. Li, Z. Wang, et al., *Ligustri Lucidi Fructus* as a traditional Chinese medicine: A review of its phytochemistry and pharmacology, Nat. Prod. Res. 29 (2015) 493–510.
[4] L. Yu, J.-X. Ren, H.-M. Nan, et al., Identification of antibacterial and antioxidant constituents of the essential oils of *Cynanchum chinense* and *Ligustrum compactum*, Nat. Prod. Res. 29 (2015) 1779–1782.
[5] L.-L. Yu, J.-T. Lou, R.-X. Wei, et al., Protective effect of Ligustri Lucidi Ait Polysaccharide against lipopolysaccharide-induced inflammatory injury of Sertoli cells in rats, Zhonghua Nan Ke Xue 24 (2018) 871–877.
[6] N. Yang, Y. Zhang, J. Guo, Preventive effect of total glycosides from *Ligustri Lucidi Fructus* against nonalcoholic fatty liver in mice, Z. Naturforsch. C. J. Biosci. 70 (2015) 237–241.
[7] C.H. Ko, W.S. Siu, C.P. Lau, et al., Osteoprotective effects of Fructus Ligustri Lucidi aqueous extract in aged ovariectomized rats, Chin. Med. 5 (2010), 39.
[8] D. Ma, A. Shan, Z. Chen, et al., Effect of *Ligustrum lucidum* and *Schisandra chinensis* on the egg production, antioxidant status and immunity of laying hens during heat stress, Arch. Anim. Nutr. 59 (2005) 439–447.
[9] Y. Zhang, L. Liu, J. Gao, et al., New secoiridoids from the fruits of *Ligustrum lucidum* Ait with triglyceride accumulation inhibitory effects, Fitoterapia 91 (2013) 107–112.
[10] Q. Wang, M. Fan, Z. Bian, et al., Extract and identify ingredient from *Ligustrum lucidum* Ait and study its effect to periodontal pathogen, Zhonghua Kou Qiang Yi Xue Za Zhi 37 (2002) 388–390.
[11] D. Hu, S. Huang, Y. Ding, et al., Specnuezhenide reduces carbon tetrachloride-induced liver injury in mice through inhibition of oxidative stress and hepatocyte apoptosis, J. Pharm. Pharmacol. 74 (2022) 191–199.
[12] J. Yang, J. Jia, Y. Yang, et al., Protective effect of specnuezhenide on islet β cell of rats with gestational diabetes mellitus, Cell. Mol. Biol. (Noisy-le-grand) 66 (2020) 60–64.
[13] C. Ma, X. Zhou, K. Xu, et al., Specnuezhenide decreases interleukin-1β-induced inflammation in rat chondrocytes and reduces joint destruction in osteoarthritic rats, Front. Pharmacol. 9 (2018), 700.
[14] J. Wu, X. Ke, W. Fu, et al., Inhibition of hypoxia-induced retinal angiogenesis by specnuezhenide, an effective constituent of *Ligustrum lucidum* Ait., through suppression of the HIF-1α/VEGF signaling pathway, Molecules 21 (2016), 1756.
[15] Y. Ding, Z. Ju, C. Ma, A validated LC-MS/MS method for the determination of specnuezhenide and salidroside in rat plasma and its application to a pharmacokinetic study, Biomed. Chromatogr. 32 (2018), e4353.
[16] S.H. Wong, J. Yu, Gut microbiota in colorectal cancer: Mechanisms of action and clinical applications, Nat. Rev. Gastroenterol. Hepatol. 16 (2019) 690–704.
[17] T.S.B. Schmidt, J. Raes, P. Bork, The human gut microbiome: From association to modulation, Cell 172 (2018) 1198–1215.
[18] R.K. Weersma, A. Zhernakova, J. Fu, Interaction between drugs and the gut microbiome, Gut 69 (2020) 1510–1519.
[19] B. Javdan, J.G. Lopez, P. Chankhamjon, et al., Personalized mapping of drug metabolism by the human gut microbiome, Cell 181 (2020) 1661–1679.e22.
[20] Y. Wang, J.W. Shou, X.Y. Li, et al., Berberine-induced bioactive metabolites of the gut microbiota improve energy metabolism, Metabolism 70 (2017) 72–84.
[21] W. Yoo, J.K. Zieba, N.J. Foegeding, et al., High-fat diet-induced colonocyte dysfunction escalates microbiota-derived trimethylamine *N*-oxide, Science 373 (2021) 813–818.
[22] P.D. Cani, M. Van Hul, C. Lefort, et al., Microbial regulation of organismal energy homeostasis, Nat. Metab. 1 (2019) 34–46.
[23] A. Koh, A. Molinaro, M. Ståhlman, et al., Microbially produced imidazole propionate impairs insulin signaling through mTORC1, Cell 175 (2018) 947–961.e17.
[24] I. Mogilnicka, M. Ufnal, Gut mycobiota and fungal metabolites in human homeostasis, Curr. Drug Targets 20 (2019) 232–240.
[25] A. Kombrink, A. Tayyrov, A. Essig, et al., Induction of antibacterial proteins and peptides in the coprophilous mushroom *Coprinopsis cinerea* in response to bacteria, ISME J. 13 (2019) 588–602.
[26] M. Fernández de Ullivarri, S. Arbulu, E. Garcia-Gutierrez, et al., Antifungal peptides as therapeutic agents, Front. Cell. Infect. Microbiol. 10 (2020), 105.
[27] J.M. Peirce, K. Alviña, The role of inflammation and the gut microbiome in depression and anxiety, J. Neurosci. Res. 97 (2019) 1223–1241.
[28] M. Rebersek, Gut microbiome and its role in colorectal cancer, BMC Cancer 21 (2021), 1325.
[29] K. Hezaveh, R.S. Shinde, A. Klötgen, et al., Tryptophan-derived microbial metabolites activate the aryl hydrocarbon receptor in tumor-associated macrophages to suppress anti-tumor immunity, Immunity 55 (2022) 324–340.e8.
[30] T. Vatanen, E.A. Franzosa, R. Schwager, et al., The human gut microbiome in early-onset type 1 diabetes from the TEDDY study, Nature 562 (2018) 589–594.

[31] Y. Wang, Q. Tong, S.-R. Ma, et al., Oral berberine improves brain dopa/dopamine levels to ameliorate Parkinson's disease by regulating gut microbiota, Signal Transduct. Target. Ther. 6 (2021), 77.
[32] R.L. Siegel, K.D. Miller, H.E. Fuchs, et al., Cancer statistics, 2022, CA, Cancer J. Clin. 72 (2022) 7–33.
[33] C. Eng, A.A. Jácome, R. Agarwal, et al., A comprehensive framework for early-onset colorectal cancer research, Lancet Oncol. 23 (2022) e116–e128.
[34] M. Ahmed, Colon cancer: A clinician's perspective in 2019, Gastroenterology Res. 13 (2020) 1–10.
[35] E.M. Park, M. Chelvanambi, N. Bhutiani, et al., Targeting the gut and tumor microbiota in cancer, Nat. Med. 28 (2022) 690–703.
[36] V. Matson, C.S. Chervin, T.F. Gajewski, Cancer and the microbiome-influence of the commensal microbiota on cancer, immune responses, and immunotherapy, Gastroenterology 160 (2021) 600–613.
[37] B. Aykut, S. Pushalkar, R. Chen, et al., The fungal mycobiome promotes pancreatic oncogenesis via activation of MBL, Nature 574 (2019) 264–267.
[38] R. Feng, Z.-X. Zhao, S.-R. Ma, et al., Gut microbiota-regulated pharmacokinetics of berberine and active metabolites in beagle dogs after oral administration, Front. Pharmacol. 9 (2018), 214.
[39] L. Pan, H. Yu, J. Fu, et al., Berberine ameliorates chronic kidney disease through inhibiting the production of gut-derived uremic toxins in the gut microbiota, Acta Pharm. Sin. B 13 (2023) 1537–1553.
[40] Z.-W. Zhang, C.-S. Gao, H. Zhang, et al., *Morinda officinalis* oligosaccharides increase serotonin in the brain and ameliorate depression via promoting 5-hydroxytryptophan production in the gut microbiota, Acta Pharm. Sin. B 12 (2022) 3298–3312.
[41] R. Chen, Y. Xu, P. Wu, et al., Transplantation of fecal microbiota rich in short chain fatty acids and butyric acid treat cerebral ischemic stroke by regulating gut microbiota, Pharmacol. Res. 148 (2019), 104403.
[42] Y. He, L. Fu, Y. Li, et al., Gut microbial metabolites facilitate anticancer therapy efficacy by modulating cytotoxic $CD8^+$ T cell immunity, Cell Metab. 33 (2021) 988–1000.e7.
[43] H.J. Kim, C.M. Moon, J.L. Kang, et al., Aging effects on the diurnal patterns of gut microbial composition in male and female mice, Korean J. Physiol. Pharmacol. 25 (2021) 575–583.
[44] L. Hu, L. Jin, D. Xia, et al., Nitrate ameliorates dextran sodium sulfate-induced colitis by regulating the homeostasis of the intestinal microbiota, Free Radic. Biol. Med. 152 (2020) 609–621.
[45] H.M. Kakelar, A. Barzegari, J. Dehghani, et al., Pathogenicity of *Helicobacter pylori* in cancer development and impacts of vaccination, Gastric Cancer 22 (2019) 23–36.
[46] S. Albhaisi, A. Shamsaddini, A. Fagan, et al., Gut microbial signature of hepatocellular cancer in men with cirrhosis, Liver Transpl. 27 (2021) 629–640.
[47] C.Y. Huang, M.C. Wang, *Clostridium perfringens* bacteremia associated with colorectal cancer in an elderly woman, Turk. J. Gastroenterol. 31 (2020) 960–961.
[48] S.C. Chang, M.H. Shen, C.Y. Liu, et al., A gut butyrate-producing bacterium *Butyricicoccus pullicaecorum* regulates short-chain fatty acid transporter and receptor to reduce the progression of 1,2-dimethylhydrazine-associated colorectal cancer, Oncol. Lett. 20 (2020), 327.
[49] A. Badgeley, H. Anwar, K. Modi, et al., Effect of probiotics and gut microbiota on anti-cancer drugs: Mechanistic perspectives, Biochim. Biophys. Acta Rev. Cancer 1875 (2021), 188494.
[50] T.T. Jiang, T.-Y. Shao, W.X.G. Ang, et al., Commensal fungi recapitulate the protective benefits of intestinal bacteria, Cell Host Microbe 22 (2017) 809–816.
[51] P. Venkatachalam, V.K. Nadumane, Modulation of Bax and Bcl-2 genes by secondary metabolites produced by *Penicillium rubens JGIPR9* causes the apoptosis of cancer cell lines, Mycology 12 (2019) 69–81.
[52] R. Pérez-Torrado, A. Querol, Opportunistic strains of *Saccharomyces cerevisiae*: A potential risk sold in food products, Front. Microbiol. 6 (2016), 1522.
[53] S. Shah, A. Locca, Y. Dorsett, et al., Alterations of the gut mycobiome in patients with MS, eBioMedicine 71 (2021), 103557.
[54] A.H. Groll, T.J. Walsh, Uncommon opportunistic fungi: New nosocomial threats, Clin. Microbiol. Infect. 7 (2001) 8–24.
[55] L. Rong, Z. Li, X. Leng, et al., Salidroside induces apoptosis and protective autophagy in human gastric cancer AGS cells through the PI3K/Akt/mTOR pathway, Biomed. Pharmacother. 122 (2020), 109726.
[56] H. Shang, S. Wang, J. Yao, et al., Salidroside inhibits migration and invasion of poorly differentiated thyroid cancer cells, Thorac. Cancer 10 (2019) 1469–1478.
[57] S.-Y. Ding, M.-T. Wang, D.-F. Dai, et al., Salidroside induces apoptosis and triggers endoplasmic reticulum stress in human hepatocellular carcinoma, Biochem. Biophys. Res. Commun. 527 (2020) 1057–1063.
[58] X. Zhang, L. Xie, J. Long, et al., Salidroside: A review of its recent advances in synthetic pathways and pharmacological properties, Chem. Biol. Interact. 339 (2021), 109268.
[59] M.B. Plotnikov, T.M. Plotnikova, Tyrosol as a neuroprotector: Strong effects of a "weak" antioxidant, Curr. Neuropharmacol. 19 (2021) 434–448.
[60] D.H. Lee, Y.J. Kim, M.J. Kim, et al., Pharmacokinetics of tyrosol metabolites in rats, Molecules 21 (2016), 128.
[61] Z.-X. Zhao, J. Fu, S.-R. Ma, et al., Gut-brain axis metabolic pathway regulates antidepressant efficacy of albiflorin, Theranostics 8 (2018) 5945–5959.
[62] J.-B. Yu, Z.-X. Zhao, R. Peng, et al., Gut microbiota-based pharmacokinetics and the antidepressant mechanism of paeoniflorin, Front. Pharmacol. 10 (2019), 268.
[63] M.L.Y. Wan, V.A. Co, H. El-Nezami, Dietary polyphenol impact on gut health and microbiota, Crit. Rev. Food Sci. Nutr. 61 (2021) 690–711.
[64] Q. Gu, C. Xia, N. Liu, et al., *Lactobacillus plantarum* ZJ316 alleviates ulcerative colitis by inhibiting inflammation and regulating short-chain fatty acid levels and the gut microbiota in a mouse model, Food Funct. 14 (2023) 3982–3993.
[65] Y. Yao, L. Yan, H. Chen, et al., *Cyclocarya paliurus* polysaccharides alleviate type 2 diabetic symptoms by modulating gut microbiota and short-chain fatty acids, Phytomedicine 77 (2020), 153268.
[66] A. Braune, M. Gütschow, M. Blaut, An NADH-dependent reductase from *Eubacterium ramulus* catalyzes the stereospecific heteroring cleavage of flavanones and flavanonols, Appl. Environ. Microbiol. 85 (2019), e01233-19.
[67] P.M. Smith, M.R. Howitt, N. Panikov, et al., The microbial metabolites, short-chain fatty acids, regulate colonic T_{reg} cell homeostasis, Science 341 (2013) 569–573.
[68] M. Vestergaard, H. Ingmer, Antibacterial and antifungal properties of resveratrol, Int. J. Antimicrob. Agents 53 (2019) 716–723.
[69] X. Zhang, Y. Han, W. Huang, et al., The influence of the gut microbiota on the bioavailability of oral drugs, Acta Pharm. Sin. B 11 (2021) 1789–1812.
[70] Z. Zhao, F. Li, J. Ning, et al., Novel compound FLZ alleviates rotenoneinduced PD mouse model by suppressing TLR4/MyD88/NF-kappa B pathway through microbiotaegutebrain axis, Acta Pharm. Sin. B 11 (2021) 2859–2879.
[71] Y. He, J. Ma, X. Fan, et al., The key role of gut-liver axis in pyrrolizidine alkaloid-induced hepatotoxicity and enterotoxicity, Acta Pharm. Sin. B 11 (2021) 3820–3835.